biomolecules

MDPI

Article

Cardiomyocyte FGFR1 Signaling Attenuates Adverse Ventricular Remodeling and Preserves Cardiac Function

Nasser H. Alatawi [1], Sanskruti R. Gare [1], Min Fang [1], Yihua Han [1], Oveena Fonseka [1], Jiayan Zhang [1], Xinyi Chen [1], Riham R. E. Abouleisa [2], Tao Wang [1], Sabu Abraham [1], Bernard D. Keavney [1,3], Elizabeth J. Cartwright [1], Tamer M. A. Mohamed [1,3,4], Wei Liu [1,*,†]

[1] Faculty of Biology, Medicine and Health, The University of Manchester, Manchester M13 9PL, UK; xinyi.chen-2@manchester.ac.uk (X.C.); tao.wang@manchester.ac.uk (T.W.)
[2] Surgery Department, Baylor College of Medicine, 1 Baylor Plaza, MS390, Houston, TX 77030, USA; riham.abouleisa@bcm.edu
[3] Manchester Heart Centre, Manchester University NHS Foundation Trust, Manchester Academic Health Science Centre, M13 9WL, Manchester, UK
[4] Institute of Molecular Cardiology, University of Louisville, 550 S. Jackson St., Louisville, KY 40202, USA
* Correspondence: wei.liu@manchester.ac.uk
† Core Technology Facility, Faculty of Biology, Medicine and Health, University of Manchester, Manchester M13 9WU, UK.

Abstract

Background: Heart failure (HF) is characterized by progressive adverse remodeling. However, the underlying molecular mechanisms governing the progression of pathological remodeling and ventricular dysfunction remain incompletely defined. Fibroblast growth factor receptor 1 (FGFR1) regulates growth factor signaling in the heart, yet its role in HF is limited. **Methods**: Proteomic and transcriptomic analyses were performed on left ventricular tissue from patients with HF to identify dysregulated remodeling pathways. FGFR1 expression and protein kinase B (AKT) signaling were examined in human hearts, in mice subjected to chronic isoprenaline infusion, and in cardiomyocyte-specific FGFR1 knockout (FGFR1^{cKO}) mice. In vitro studies were conducted in neonatal rat cardiomyocytes (NRCMs) and rat myoblasts (H9C2) using si*RNA*-mediated FGFR1 knockdown and stimulating AKT phosphorylation by the specific activator SC-79 under isoprenaline-induced β-adrenergic stress. Genetic restoration of FGFR1 was achieved using adeno-associated viral subtype 9 (AAV9) delivery of FGFR1 after the onset of remodeling, followed by echocardiographic, histological, and molecular analyses. **Results**: Human HF hearts exhibited broad dysregulation of remodeling pathways. Notably, AKT signaling was markedly suppressed. Reduced FGFR1 expression was accompanied by decreased AKT phosphorylation in human HF hearts. Consistently, chronic isoprenaline stress reduced cardiac FGFR1 expression in vivo and in vitro. Cardiomyocyte-specific FGFR1 deletion exacerbated systolic dysfunction and promoted ventricular dilation. Mechanistically, FGFR1 deficiency suppressed AKT activation, which contributed to cardiac pathological remodeling upon isoprenaline stress. In cardiomyocytes with FGFR1 knockdown, cardiomyocyte injury and maladaptive transcriptional responses were amplified under β-adrenergic stress. Of note, these detrimental effects were rescued by pharmacological activation of AKT using its activator, SC-79. Therapeutically, genetic FGFR1 re-establishment attenuated cardiac pathological remodeling and restored systolic function under longer-term isoprenaline stress, at least partially through maintenance of AKT activation. **Conclusions**: The current study has demonstrated that cardiac FGFR1 signaling exhibits cardioprotective potential that mitigates adverse ventricular remodeling and rescues cardiac

Academic Editor: Mohsin Saleet Jafri

Received: 21 September 2026
Revised: 22 October 2026
Accepted: 2 November 2026
Published: 7 November 2026

Copyright: © 2026 by the authors. Licensee MDPI, Basel, Switzerland. This article is an open access article distributed under the terms and conditions of the Creative Commons Attribution (CC BY) license.

function under pathological stress. Therefore, targeting FGFR1 signaling represents a potential strategy to prevent pathological remodeling and HF.

Keywords: FGFR1; HF; AKT; cardiac remodeling; isoprenaline

1. Introduction

Heart failure (HF) remains a leading cause of morbidity and mortality worldwide despite substantial advances in pharmacological and device-based therapies [1,2]. Progressive deterioration of cardiac function in HF is driven largely by maladaptive ventricular remodeling, a complex process characterized by cardiomyocyte hypertrophy, chamber dilation, fibrotic tissue formation, cell death, and impaired contractile performance [3]. Although neurohormonal blockade and guideline-directed therapies can slow the rate of disease progression, many patients continue to experience development of adverse remodeling and vulnerable transition to HF [4], underscoring the need to advance understanding of the molecular pathogenic pathways that participate in the onset and progression of cardiac remodeling and HF.

Among the intracellular signaling networks regulating myocardial growth and survival, the protein kinase B (AKT) pathway has emerged as a central cardioprotective axis under both physiological and pathological conditions [5,6]. Early studies in cardiac cells demonstrated that AKT activation promotes cardiomyocyte survival by inhibiting apoptotic signaling and preserving mitochondrial integrity, as shown in neonatal and adult cardiomyocytes exposed to hypoxia or oxidative stress in vitro [5,7–9]. Consistent with these findings, activation of AKT has been shown to protect cardiomyocytes from oxygen-glucose deprivation and reoxygenation-induced cell death [10]. In vivo evidence from genetic overexpression models similarly demonstrates that enhanced AKT signaling limits myocardial injury, reduces cardiomyocyte apoptosis, and decreases infarct size following ischemia–reperfusion injury or myocardial infarction, resulting in improved cardiac function [6,8]. While AKT activation is widely recognized as cardioprotective in acute stress settings, the treatment potential of targeting it and its regulators remains incompletely understood.

Fibroblast growth factor receptor 1 (FGFR1) is a transmembrane receptor tyrosine kinase that regulates cell survival, proliferation, and stress adaptation through activation of multiple downstream signaling cascades. In the heart, FGFR1 contributes to the development and differentiation of cardiomyocytes, highlighting its importance in cardiac growth and maturation [11]. Under diabetic stress conditions, FGFR1 activation has been shown to enhance wound-healing responses and suppress the secretion of inflammatory cytokines in cardiomyocytes in vitro, suggesting a role in protecting cardiac cells from metabolic stress [12]. In addition, endothelial FGFR1 plays an important role in maintaining vascular homeostasis, and its loss promotes TGF-β-induced fibroblast activation, leading to increased fibrosis and extracellular matrix deposition in the diabetic heart [13]. Furthermore, FGF21-mediated FGFR1 signaling has been shown to protect against pathological cardiac hypertrophy by promoting mitophagy and maintaining mitochondrial quality control in pressure overload models such as transverse aortic constriction (TAC) [14]. Conversely, deficiency of both FGFR1 and FGFR2 in cardiomyocytes exacerbates apoptosis, fibrosis, and ventricular dysfunction during the acute phase following ischemia–reperfusion injury, partly through suppression of pro-survival signaling pathways [15]. Despite these findings, the functional role of FGFR1 signaling in HF remains poorly defined.

https://doi.org/10.3390/biom16111621

In the present study, we have demonstrated the role of FGFR1 signaling as a regulator of cardiac remodeling and ventricular function under β-adrenergic stress. Integrated analyses of human failing myocardium revealed coordinated dysregulation of remodeling-associated pathways characterized by suppression of AKT signaling alongside reduced FGFR1 expression, suggesting a potential upstream regulatory relationship. Functional studies demonstrate that loss of FGFR1 exacerbates systolic dysfunction and promotes adverse pathological remodeling, including increased fibrosis and cardiomyocyte apoptosis, during isoprenaline-induced stress, identifying FGFR1 as a critical mediator of cardioprotective signaling. Mechanistically, FGFR1 maintains myocardial homeostasis, at least in part, through regulation of AKT activity, and restoration of FGFR1 signaling mitigates maladaptive remodeling and preserves cardiac function.

Collectively, these findings establish FGFR1 as a potential upstream regulator of AKT-dependent cardioprotection and highlight the FGFR1-AKT signaling axis as a therapeutic target for mitigating maladaptive remodeling and HF progression.

2. Materials and Methods

2.1. Data and Materials Availability

The data presented in this study are available upon request from the corresponding author because the data are not publicly available under the study's data-sharing arrangements.

2.2. Human Samples

Human hearts were either purchased from Asterand (BioIVT, Bioivt.com, sale ID 224622; Asterand obtained ethical approval and consent following the United Kingdom Human Tissue Authority regulations) or obtained from the transplantation network in the USA (UNOS) from de-identified donors and we have obtained approval from the Institutional Review Board of Baylor College of Medicine for non-human subject research (protocol number H-53940 (30/06/2023). All experimental procedures performed on human samples were approved by the University of Manchester Ethics Committees and in agreement with the Declaration of Helsinki (12172, the Human Tissue Authority, 18 September 2020).

2.3. Animal Studies

All animal experiments were conducted in accordance with the United Kingdom Animals (Scientific Procedures) Act 1986 and were approved by the University of Manchester Ethics Committee under the PPL license PP0172073 (23/09/2025) and PA8E7CA4E (29 September 2020). Cardiomyocyte-specific FGFR1 knockout mice ($FGFR1^{cKO}$) were generated for functional studies. Floxed littermates ($FGFR1^{Flox}$) served as controls. On the other hand, after 2 weeks of isoprenaline infusion, wild-type (WT) mice were randomly allocated to receive either AAV9-cTnT-*Fgfr1* or AAV9-cTnT-*Gfp* by a computer-generated random sequence.

2.4. Induction of β-Adrenergic Stress

Cardiac β-adrenergic stress was induced via mini-osmotic pump implantation (Alzet) delivering isoprenaline at 10 mg/kg/day for 2–4 weeks, as described previously [16].

2.5. In Vitro Models

Neonatal rat cardiomyocytes (NRCMs) were isolated and cultured as previously described [17]. H9C2 cells were maintained in DMEM supplemented with 10% (*v*/*v*) heat-inactivated fetal bovine serum (FBS), 100 μg/mL streptomycin, and 100 U/mL penicillin at 37 °C in 5% CO_2. β-adrenergic stress was mimicked in vitro using isoprenaline (10 μM) for 8–16 h as stipulated in the Results.

2.6. Statistics

Data are shown as bar or dot plots representing mean ± SEM. Normality was assessed using the Shapiro–Wilk test. Normally distributed data were analyzed by one- or two-way ANOVA with post hoc tests, while two-group comparisons utilized two-tailed Student's unpaired *t*-tests. Non-parametric tests were applied for skewed data or $n < 5$, unless otherwise stated. If the data were not normally distributed, non-parametric tests (equivalent to one-way ANOVA and Student's *t*-test), such as the Kruskal–Wallis test or the Mann–Whitney U test, were used. Analyses were performed in GraphPad Prism 10, with $p < 0.05$ considered statistically significant.

3. Results

3.1. FGFR1 and AKT Signaling Is Dysregulated in Human and Experimental HF

To identify molecular pathways dysregulated in human HF, we performed gene ontology (GO) pathway enrichment analysis of proteomic data generated by liquid chromatography–tandem mass spectrometry from failing and non-failing human left ventricular tissue (Appendix A.2). Among 496 altered proteins ($p < 0.05$), GO analysis revealed enrichment ($p < 0.05$ Reactome) of multiple cardiac remodeling-associated pathways, including apoptotic processes, oxidative stress responses, and hypertrophic and angiogenic signaling pathways (Figure 1A). These findings indicate that HF is characterized by coordinated disruption of pathways regulating myocardial structure and adaptive signaling. To further define transcriptional changes associated with these proteomic alterations, we analyzed RNA sequencing data from the same cohort (from overlapping donors). GO analysis ($P_{adj.} < 0.05$ Reactome) of the 2025 altered genes ($p < 0.05$) identified the protein kinase B (AKT) signaling pathway as one of the most prominently dysregulated pathways, along with growth factor-mediated survival and hypertrophic signaling, in failing hearts (Figure 1B). Consistent with this, levels of phosphorylated AKT (pAKT) at Ser473 were significantly reduced in failing human hearts compared with non-failing controls, whereas total AKT expression remained largely unchanged (Figure 1C,D), indicating reduced AKT activation in HF.

Given the prominent disruption of AKT signaling in failing hearts, we next sought to identify upstream regulators responsible for AKT activation. Fibroblast growth factor receptors (FGFRs) have been implicated as key regulators of AKT signaling in development and cancer [18]. Considering the abundant expression of FGFR1 in cardiomyocytes [14], we therefore examined cardiac FGFR1 expression. Immunoblot analysis demonstrated a significant reduction in FGFR1 expression in left ventricular tissue from HF patients compared with non-failing controls (Figure 1E,F). To determine whether FGFR1 downregulation is recapitulated in experimental models of HF, we assessed its expression in mice subjected to isoprenaline administration, a well-established model of β-adrenergic-induced cardiac remodeling in HF [19]. Consistent with the human data, FGFR1 expression was significantly reduced in hearts from isoprenaline-treated mice compared with controls after 2 weeks of minipump infusion (Figure 1G,H). Similarly, in vitro exposure of NRCMs to isoprenaline resulted in a marked decrease in FGFR1 expression after 16 h

(Figure 1I,J), indicating that β-adrenergic stress directly suppresses FGFR1 expression at the cellular level.

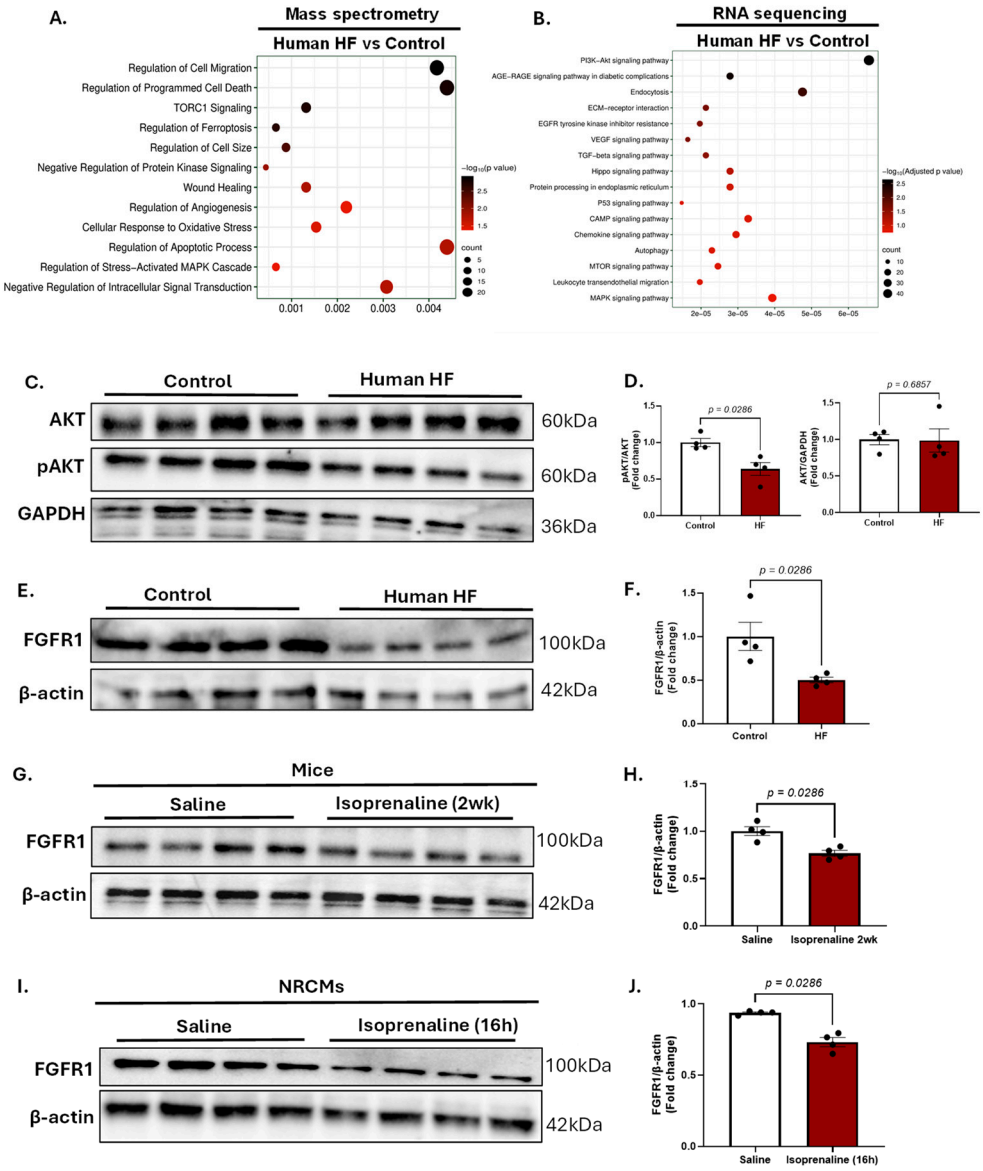


Figure 1. Cardiac remodeling pathways and FGFR1 and AKT signaling are dysregulated in human HF and experimental stress models. (**A**) Gene Ontology (GO) pathway enrichment analyses ($p < 0.05$ Reactome pathways) of the altered proteins ($p < 0.05$) identified via liquid chromatography–tandem mass spectrometry of human heart failure (HF) versus non-failing control left ventricular tissue ($n = 8$ for control and $n = 7$ for HF). (**B**) GO pathway enrichment analyses (*Padj.* < 0.05 Reactome) of the altered genes ($p < 0.05$) identified via RNA sequencing in human failing hearts compared to non-failing human hearts ($n = 4$ for control group and $n = 6$ for HF group). (**C**,**D**) Representative immunoblots and quantification showing phosphorylated AKT (pAKT Ser473) and total AKT expression in failing human hearts vs. non-failing ($n = 4$ hearts/group). GAPDH was used as the loading control. pAKT/AKT ratios normalized to GAPDH are shown. (**E**,**F**) Representative immunoblots and quantification showing FGFR1 expression in failing human hearts ($n = 4$ hearts/group). (**G**,**H**) Representative immunoblots and quantification showing FGFR1 expression in mice after 2 weeks of isoprenaline infusion ($n = 4$ hearts/group). (**I**,**J**) Representative immunoblots and quantification showing FGFR1 expression in neonatal rat cardiomyocytes (NRCMs) after 16 h of isoprenaline treatment ($n = 4$ cells/group). Beta actin (β-actin) was used as the loading control for (**E**,**G**,**I**). Data are

presented as mean ± SEM. Statistical significance (*p* values shown in the panel) was assessed using the Mann–Whitney U test (**D**,**H**,**F**,**J**).

Collectively, these data demonstrate that cardiac remodeling pathways are markedly dysregulated in HF. Reduced FGFR1 expression and impaired AKT signaling are concomitant with cardiac pathological remodeling in both human disease and experimental mouse models.

3.2. Cardiomyocyte FGFR1 Deletion Exacerbates Cardiac Dysfunction Under Isoprenaline Stress

To determine whether the loss of cardiomyocyte FGFR1 during pathological β-adrenergic stress causatively relates to the onset and progression of cardiac dysfunction, we subjected cardiomyocyte-specific *Fgfr1* knockout mice ($FGFR1^{cKO}$) and floxed control littermates ($FGFR1^{Flox}$, Figure S1) to isoprenaline infusion using osmotic minipumps for 2 weeks, followed by echocardiographic assessment (Figure 2A). The 2-week time point was selected based on our observation that endogenous FGFR1 expression is reduced after 2 weeks of isoprenaline treatment (Figure 1G,H), thereby allowing evaluation of the effects of FGFR1 loss on cardiac remodeling using the $FGFR1^{cKO}$ model.

Gross examination of cardiac morphology revealed cardiac enlargement in isoprenaline-treated mice compared with saline-treated controls in both genotypes (Figure 2B). Quantitative analyses showed that heart weight (HW) and the heart weight-to-tibia length (HW/TL) ratio were significantly increased following isoprenaline infusion in both $FGFR1^{Flox}$ controls and $FGFR1^{cKO}$ mice (Figure 2C,D; Table S1). However, no significant differences in HW or HW/TL were observed between genotypes under isoprenaline stress (Figure 2C,D; Table S1), indicating that cardiomyocyte FGFR1 deletion does not further augment heart gross weight.

Despite similar increases in heart mass, echocardiographic analysis revealed pronounced differences in ventricular remodeling and function between genotypes. Isoprenaline treatment induced a significant increase in posterior wall thickness during diastole (dPW) and systole (sPW) in $FGFR1^{Flox}$ mice, consistent with an adaptive hypertrophic response to β-adrenergic stress (Figure 2E; Table S1). In contrast, this compensatory wall thickening was blunted in $FGFR1^{cKO}$ mice, resulting in significantly reduced dPW and sPW compared with $FGFR1^{Flox}$ controls under isoprenaline stress for 2 weeks (Figure 2E; Table S1). Left ventricular internal diameter in diastole (dD) and systole (sD) were not significantly altered by isoprenaline treatment in control mice compared with the saline treatment group; however, loss of FGFR1 exhibited a significant increase in dD and sD following isoprenaline infusion, indicating ventricular dilation and adverse chamber remodeling (Figure 2F; Table S1). Corresponding to these structural changes, isoprenaline-treated $FGFR1^{cKO}$ mice exhibited significantly reduced ejection fraction (Figure 2G; Table S1) and fractional shortening (Figure 2H; Table S1) compared with floxed controls, indicating impaired systolic performance. Assessment of left ventricular outflow tract hemodynamics also revealed differential effects of isoprenaline stress on aortic flow. In floxed mice, aortic maximal velocity (V_{max}) was preserved despite 2 weeks of isoprenaline stimulation, whereas $FGFR1^{cKO}$ mice exhibited a significant reduction in V_{max}, suggesting impaired systolic ejection. Furthermore, aortic flow gradient was decreased in floxed mice following isoprenaline infusion, which was further exacerbated in $FGFR1^{cKO}$ mice (Figure 2I,J; Table S1), consistent with compromised forward flow and severe functional deterioration in the absence of FGFR1.

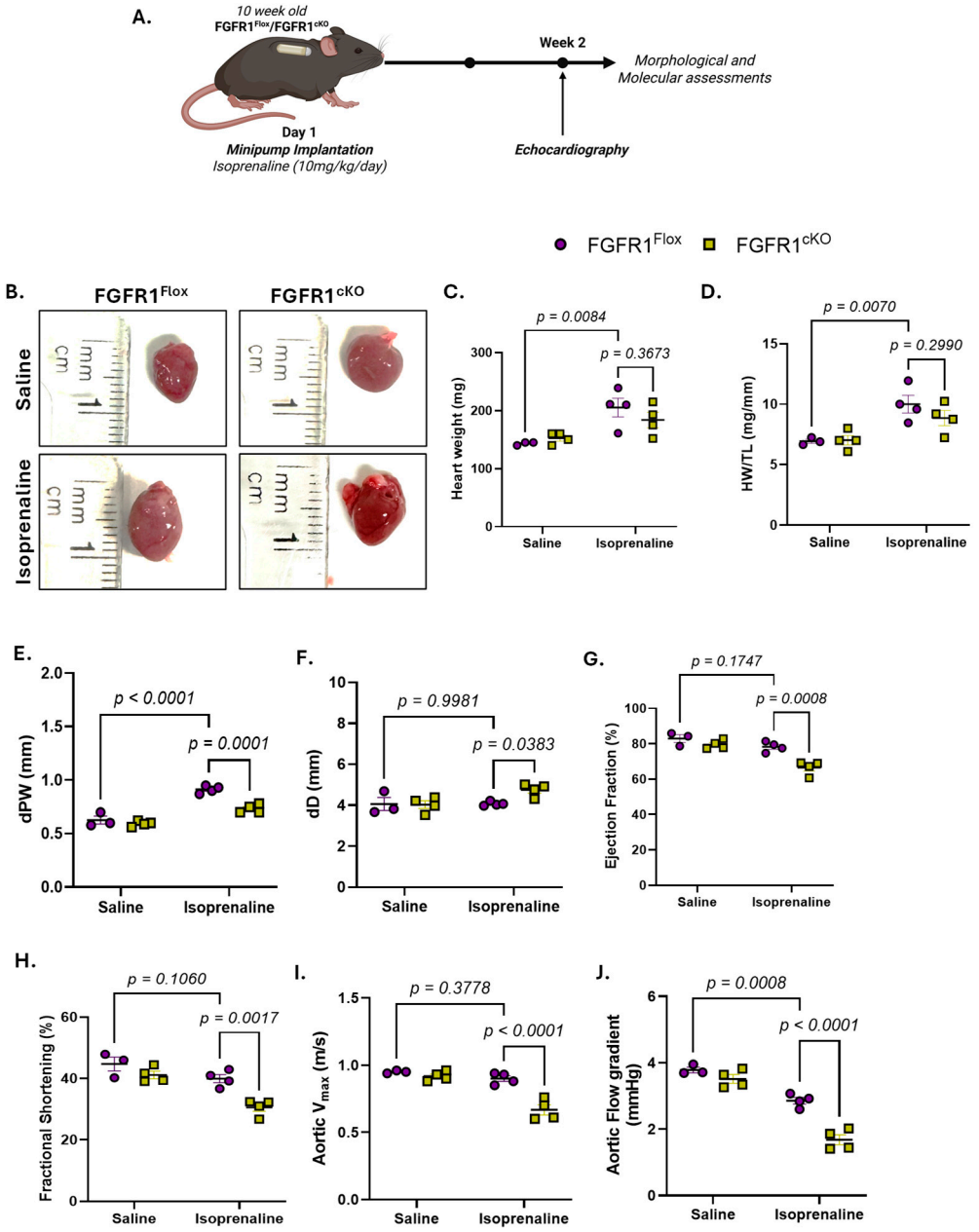


Figure 2. Cardiomyocyte FGFR1 deletion exacerbates ventricular dysfunction under isoprenaline stress. (**A**) Schematic of the experimental design illustrating a 2-week isoprenaline infusion followed by echocardiographic assessment in 10-week-old cardiomyocyte-specific FGFR1 knockout (FGFR1^{cKO}) and floxed (FGFR1^{Flox}) control male mice. (**B**) Representative images of excised hearts from saline- and isoprenaline-treated floxed and FGFR1 knockout mice (ruler shown, 1 cm). (**C**,**D**) Quantification of (**C**) heart weight (HW) and (**D**) HW/tibia length (HW/TL) ratios in FGFR1^{Flox} and FGFR1^{cKO} hearts receiving saline or isoprenaline administration (n = 3–4 mouse hearts/group). (**E**–**J**) Functional echocardiographic parameters in male FGFR1^{Flox} and FGFR1^{cKO} littermates following saline or isoprenaline administration. (**E**) Posterior wall thickness in diastole (dPW), (**F**) left ventricular internal diameter in diastole (dD), (**G**) percentage of left ventricular ejection fraction, (**H**) percentage of left ventricular fractional shortening, (**I**) aortic maximal velocity (V_{max}), and (**J**) aortic flow gradient. (n = 3–4 mice/group). Data are presented as mean ± SEM. Statistical significance (p values shown in the panel) was assessed using ordinary two-way ANOVA followed by Šidák multiple comparisons (**C**–**J**).

Together, these data demonstrate that loss of cardiomyocyte FGFR1 leads to detrimental effects on ventricular geometry and cardiac performance during chronic β-adrenergic stress.

3.3. FGFR1 Deficiency in Cardiomyocytes Worsens Maladaptive Remodeling Under Isoprenaline Stress

To investigate the molecular and histological changes underlying the functional deterioration observed in failing hearts under β-adrenergic stress due to FGFR1 deficiency, we first assessed AKT signaling. Immunoblot analysis revealed that pAKT levels at Ser473 were significantly reduced in FGFR1 knockout hearts following isoprenaline infusion (Figure 3A,B), indicating that loss of cardiomyocyte FGFR1 impairs AKT activation under stress, although total expression of AKT was comparable in the presence and absence of FGFR1 in the heart (Figure 3A,B). These findings were consistent with the results observed in human failing heart tissues (Figure 1C,D).

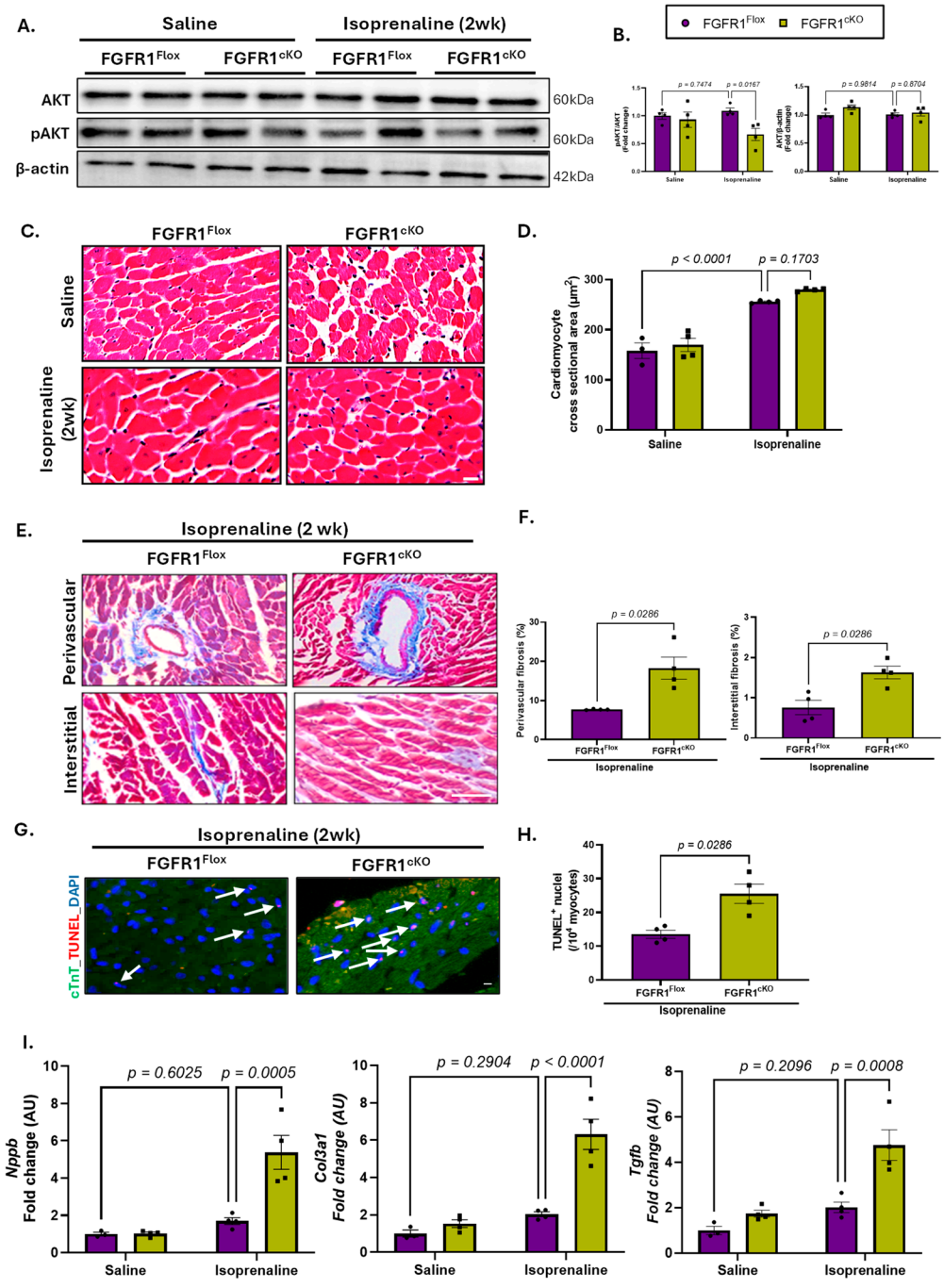


Figure 3. FGFR1 deficiency promotes pathological remodeling through suppression of AKT. (**A**,**B**) Representative immunoblots and quantification of phosphorylated AKT (pAKT Ser473) and total AKT expression in FGFR1^{Flox} and FGFR1^{cKO} hearts following saline or isoprenaline treatment (n = 4 hearts/group). Beta actin (β-actin) was used as the loading control. pAKT/AKT ratios normalized to β-actin were quantified. (**C**–**H**) Histological assessments of left ventricular tissue in FGFR1^{Flox} and FGFR1^{cKO} hearts following saline or isoprenaline treatment. (**C**,**D**) Representative H&E-stained cardiac cross-sections and corresponding quantification of cardiomyocyte cross-sectional area (CSA; scale = 20 μm), (**E**,**F**) representative Masson's Trichrome-stained heart sections showing perivascular and interstitial fibrosis along with quantification (scale = 50 μm), and (**G**,**H**) TUNEL-stained heart sections showing TUNEL-positive nuclei (red; white arrows) along with quantification graph. DAPI is shown in blue, and green represents cardiac troponin T (cTnT). (n = 4 hearts/group, scale = 10 μm). (**I**) Quantitative PCR analysis of *Nppb*, *Col3a1*, and *Tgfb1* transcripts in mouse hearts (n = 4 hearts/group). Data are presented as mean ± SEM. Statistical comparisons (indicated in each panel) were performed versus corresponding controls using ordinary two-way ANOVA followed by Šidák multiple comparisons (**B**,**D**,**I**) or Mann–Whitney test (**F**,**H**).

Hematoxylin and eosin (H&E) staining demonstrated a significant increase in cardiomyocyte cross-sectional area (CSA) in floxed mice following isoprenaline treatment (Figure 3C,D), consistent with the increase in HW (Figure 2C) and HW/TL (Figure 2D) measurements. However, no significant difference in CSA was observed between floxed and FGFR1 knockout hearts despite marked functional deterioration in the knockout mice, indicating that the exacerbated systolic dysfunction is not driven by alterations in individual cardiomyocyte size. Analysis of extracellular matrix remodeling using Masson's trichrome staining showed significantly increased interstitial as well as perivascular fibrosis in FGFR1 knockout mice following isoprenaline treatment compared with floxed controls (Figure 3E,F). In parallel, TUNEL staining indicated profound cardiomyocyte apoptosis in FGFR1^{cKO} hearts under isoprenaline stress, highlighting increased cellular injury and maladaptive remodeling (Figure 3G,H). Concomitant with these structural changes, qPCR analysis demonstrated elevated expression of genes associated with cardiac pathological remodeling. Transcript levels of *Nppb*, *Col3a1*, and *Tgfb1* were significantly higher in FGFR1^{cKO} hearts after isoprenaline infusion compared with floxed controls (Figure 3I). In addition to the above morphological changes, these data indicate enhanced pathological remodeling and profibrotic signaling in the absence of cardiomyocyte FGFR1, supporting its role in protecting the heart against decompensated remodeling under β-adrenergic stress.

Together, these findings indicate that FGFR1 disruption in cardiomyocytes is associated with cardiac adverse remodeling under β-adrenergic stress, likely through modulation of the AKT pathway.

3.4. FGFR1 Loss Promotes Pathological Remodeling Through Suppression of AKT In Vitro

Next, we examined the effects of FGFR1 loss in vitro. To do so, NRCMs and H9C2 rat myoblast cells were transfected with si*RNA* targeting FGFR1 (si*Fgfr1*) to knock down FGFR1 (Figure S2) or si*Negative* as the control, followed by 8 h of isoprenaline treatment (Figure 4A). The 8 h time point was chosen because endogenous FGFR1 levels remained unchanged at this stage (Figure S3), allowing evaluation of the effects of FGFR1 deficiency independent of stress-induced downregulation.

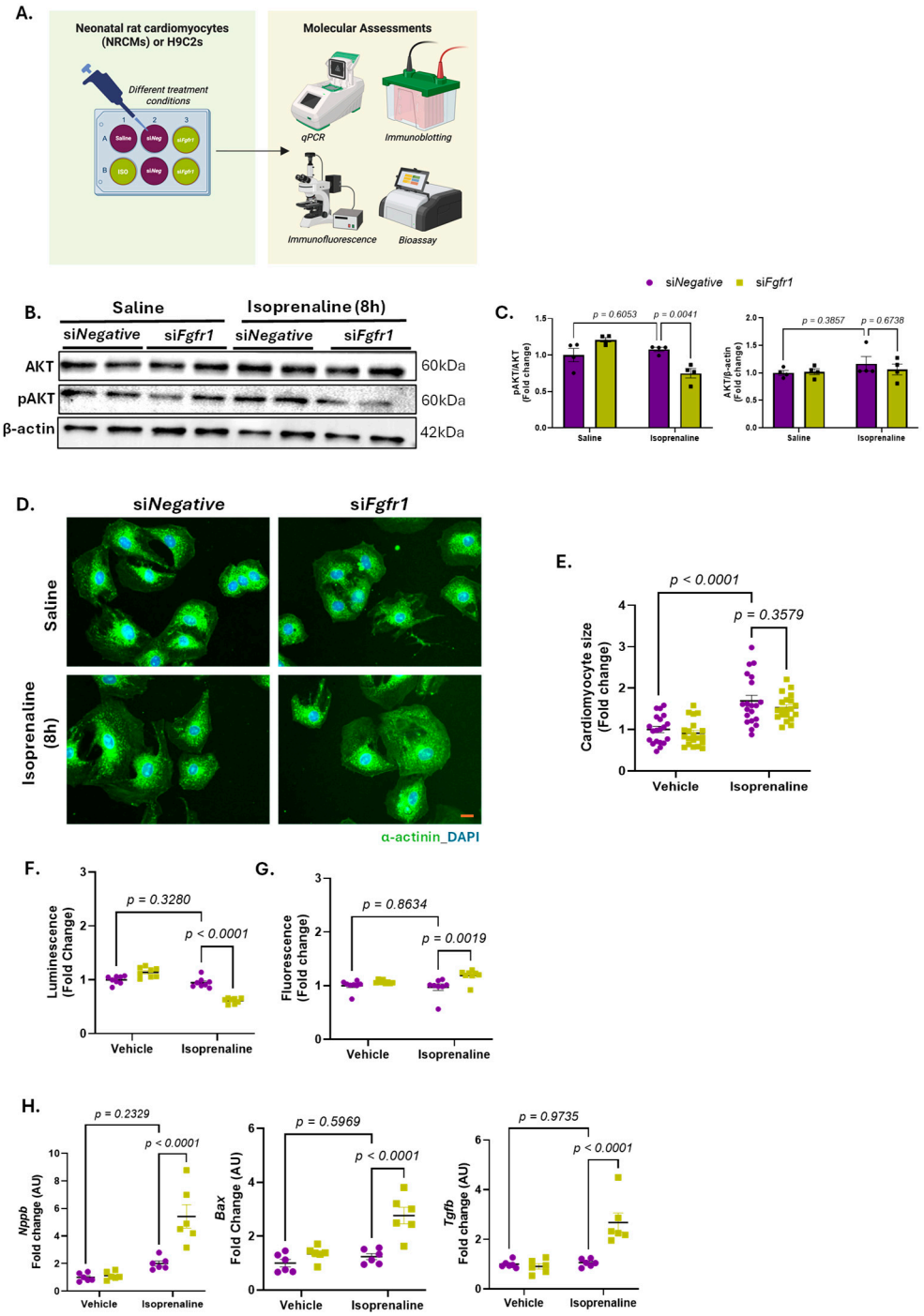


Figure 4. FGFR1 knockdown suppresses AKT signaling and exacerbates cardiomyocyte injury under isoprenaline stress. (**A**) Schematic of an in vitro experimental design. Neonatal rat cardiomyocytes (NRCMs) or rat myoblasts (H9C2s) were transfected with si*RNA* targeting FGFR1 (si*Fgfr1*) and exposed to 8 h of isoprenaline (10 μM) treatment. (**B**,**C**) Representative immunoblots and quantification of total AKT and phosphorylated AKT (Ser473) in FGFR1 knockdown under isoprenaline stress in NRCMs (n = 4 experiments/group). Beta actin (β-actin) was used as the loading control. (**D**,**E**) Immunofluorescent staining from si*Fgfr1*-treated NRCMs under saline or isoprenaline treatment showing α-actinin (green) with DAPI (blue) (scale = 20 μm). Cardiomyocyte area is quantified (n = 20 samples/group). (**F**,**G**) Quantification of (**F**) viability and (**G**) toxicity assays of NRCMs treated under similar conditions (n = 8 samples/group). (**H**) Quantitative PCR analysis of *Nppb*, *Bax*, and *Tgfb1* transcripts in NRCMs treated under similar conditions (n = 6 experiments/group). Data are presented as mean ± SEM. Statistical significance (p values shown in the panel) was assessed using ordinary two-way ANOVA followed by Šidák multiple comparisons (**C**,**E**–**H**).

https://doi.org/10.3390/biom16111621

Consistent with data obtained from humans and mice showing simultaneous reduction in FGFR1 expression and AKT activation under stress (Figures 1 and 3), immunoblot analyses revealed that FGFR1 knockdown significantly decreased phosphorylation of AKT under isoprenaline stress (Figure 4B,C), demonstrating that FGFR1, as a kinase, is likely required for AKT activation in cardiomyocytes upon the stress, albeit unaffected AKT protein expression. Furthermore, immunofluorescent staining of cardiac α-actinin on NRCMs showed that isoprenaline stimulation increased cell size in both control and FGFR1-deficient cells (Figure 4D,E), reflecting an acute hypertrophic response. However, there was no significant difference in cell size between control and FGFR1 knockdown cells under either basal or stress conditions, indicating that the exacerbated maladaptive effects of FGFR1 deficiency are not due to impaired hypertrophy at the cell level. However, FGFR1 knockdown markedly exacerbated cellular injury under isoprenaline stress. For instance, FGFR1-deficient cells exhibited significantly reduced viability and increased cytotoxicity compared with control cells following isoprenaline exposure (Figure 4F,G), indicating higher susceptibility to β-adrenergic-induced injury in the absence of FGFR1. Consistent with in vivo findings described above, qPCR analyses revealed that expression of the marker genes of pathological remodeling, including *Nppb*, *Bax* and *Tgfb1*, was significantly increased in FGFR1-deficient cells upon stimulation (Figure 4H). These findings indicate that FGFR1 deficiency amplifies cardiac stress transcriptional responses to β-adrenergic stimulation. Together, these in vitro findings indicate that loss of FGFR1 suppresses AKT activation and exacerbates cardiomyocyte injury and maladaptive gene expression under isoprenaline stress.

3.5. AKT Activation Rescues Maladaptive Responses in FGFR1-Deficient Cardiomyocytes Under Isoprenaline Stress

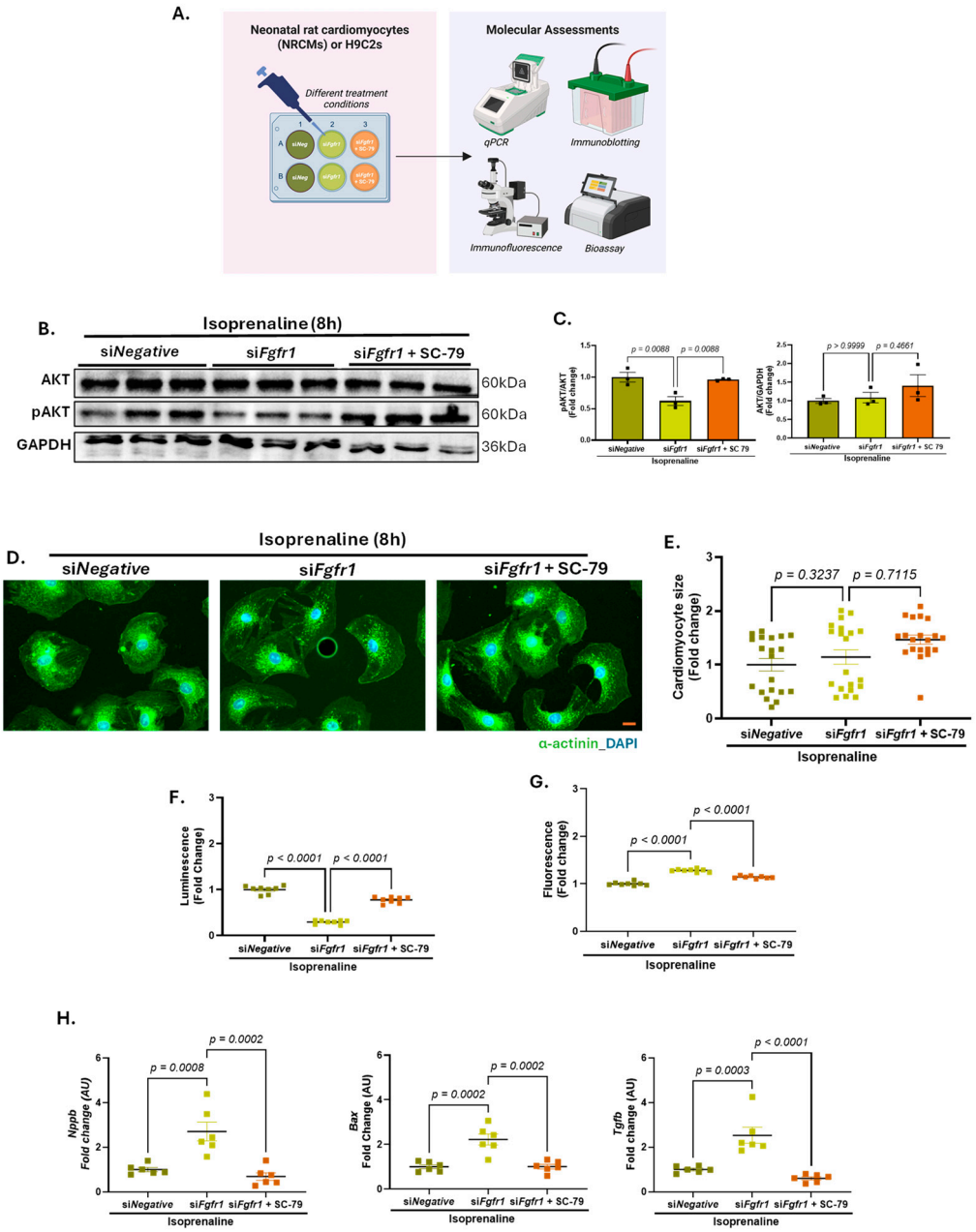
To further determine whether FGFR1 loss-induced detrimental effects on pathological remodeling are at least partially through loss of AKT activation, we attempted to restore AKT signaling in the absence of FGFR1 and assess whether this could rescue the maladaptive phenotype induced by FGFR1 deficiency. To do so, cells with FGFR1 knockdown were treated with the selective AKT activator SC-79 under stimulation with isoprenaline (Figure 5A).

In FGFR1-deficient cells exposed to isoprenaline, pAKT levels were markedly reduced. However, co-treatment with SC-79 significantly increased AKT phosphorylation, while total AKT protein levels remained unchanged (Figure 5B,C), consistent with the reported mechanism of SC-79 as a selective AKT activator that promotes AKT phosphorylation [20]. Immunofluorescence staining of α-actinin on cardiomyocytes and the quantification demonstrated that isoprenaline increased cell size across all groups as expected (Figure 5D,E). In addition, as observed in Figure 4D,E, no significant differences in cell size were detected between control and FGFR1-deficient cells. Interestingly, SC-79 treatment did not further modify hypertrophic growth, indicating that AKT activation primarily affects stress responses rather than hypertrophy in individual cardiomyocytes. On the other hand, AKT activation markedly improved cell survival in FGFR1-deficient cardiomyocytes. Moreover, SC-79 significantly increased both cell viability and reduced cytotoxicity in si*Fgfr1*-treated cells under isoprenaline stress compared with untreated FGFR1-knockdown cells (Figure 5F,G). Consistent with these protective effects, qPCR analyses further demonstrated that the elevated pathological remodeling markers observed in FGFR1-deficient cells, including *Nppb*, *Bax*, and *Tgfb1*, were significantly reduced by SC-79 treatment under isoprenaline stress (Figure 5H), indicating that activation of AKT signaling attenuates FGFR1 loss-induced injury in cardiomyocytes.

Moreover, mechanistic target of rapamycin complex 2 (mTORC2) is likely upstream of AKT and can phosphorylate AKT at Ser473 [21]. SIN1 (stress-activated protein kinase-

associated protein 1, also known as MAPKAP1, mitogen-activated protein kinase associated protein 1) is a vital scaffold subunit for mTORC2, facilitating phosphorylation of AKT [22]. To investigate whether FGFR1 modulates AKT through mTORC2, we examined phosphorylation of AKT in SIN1-deficient H9C2 cells. FGFR1-increased phosphorylation of AKT was blocked by SIN1 knockdown, although the cell size was comparable in the presence and absence of SIN1 under 8 h of isoprenaline stress (Figure 5I,J), indicating that FGFR1 activation of AKT is at least partially through mTORC2.

Together, these results demonstrate that impaired AKT signaling mediates the maladaptive effects of FGFR1 loss in cardiomyocytes. Pharmacological activation of AKT rescues cellular survival and attenuates pathological gene expression under isoprenaline stress, confirming AKT as a likely downstream mediator of FGFR1 signaling.



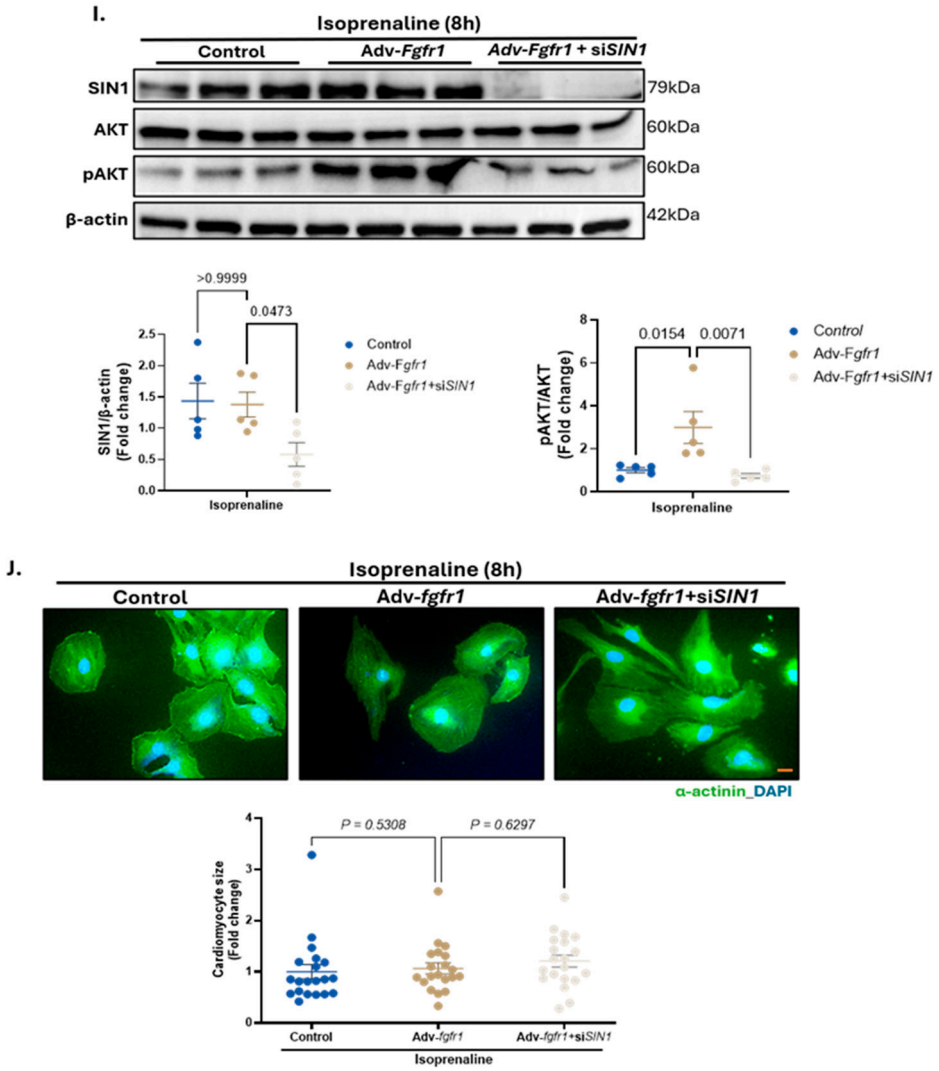


Figure 5. FGFR1 knockdown-induced maladaptive responses are reversed by AKT activation. (**A**) Experimental schematics**.** Neonatal rat cardiomyocytes (NRCMs) or cardiac myoblasts (H9C2s) were transfected with si*RNA* targeting FGFR1 (si*Fgfr1*) and exposed to isoprenaline (10 μM) for 8 h in the presence or absence of AKT activator, SC-79 (10 μM for 8 h). (**B**,**C**) Representative immunoblots and quantification of total AKT and phosphorylated AKT (Ser473) in FGFR1 knockdown NRCMs using si*Fgfr1* under isoprenaline stress (n = 3 samples/group). GAPDH was used as the loading control. pAKT/AKT ratios normalized to GAPDH are shown. (**D**,**E**) Immunofluorescent staining from si*Fgfr1*-treated NRCMs under isoprenaline stress with or without SC-79 treatment, showing α-actinin (green) with DAPI (blue) (scale = 20 μm). Cardiomyocyte area is quantified (n = 20 samples/group). (**F**,**G**) Quantification of (**F**) viability and (**G**) toxicity assays of NRCMs treated under similar conditions (n = 8 samples/group). (**H**) Quantitative PCR analysis of *Nppb*, *Bax*, and *Tgfb1* transcripts in NRCMs treated under similar conditions (n = 6 samples/group). (**I**) Representative immunoblots and quantification of SIN1, total AKT and phosphorylated AKT in FGFR1-overexpressing cells with or without SIN1. (**J**) Immunofluorescent staining of α-actinin (green) with DAPI (blue) (scale = 20 μm) and quantification of cell size. Data are presented as mean ± SEM. Statistical significance (p values shown in the panel) was assessed using ordinary one-way ANOVA followed by Holm-Šidák multiple comparisons (**C**,**F**–**H**,**I**), or Kruskal–Wallis with Dunn's multiple comparison test (**E**,**J**).

3.6. FGFR1 Restoration Ameliorates Isoprenaline Stress-Induced Cardiac Dysfunction

To evaluate the effects of FGFR1 re-expression on isoprenaline-induced cardiac dysfunction, mice received cardiac-specific FGFR1 overexpression after 2 weeks of isoprenaline stimulation, followed by assessment after 2 additional weeks (Figure 6A; Table S2A,B). FGFR1 overexpression was achieved using an adeno-associated virus serotype 9 (AAV9) vector driven by the cardiomyocyte-specific cTnT promoter (AAV9-*Fgfr1*). Control mice received AAV9-Green fluorescent protein (AAV9-*Gfp*) treatment. Similar cardiac morphology was observed between AAV9-*Fgfr1*-treated and control groups under isoprenaline stress (Figure 6B). In addition, HW and HW/TL ratios remained unaltered by FGFR1 overexpression (Figure 6C,D; Table S2B). Wall thickness (dPW and sPW) and LV internal diameter (dD and sD) were reduced following FGFR1 overexpression in comparison to the control group (Figure 6E,F; Table S2B), indicating attenuation of cardiac hypertrophy and ventricular dilation.

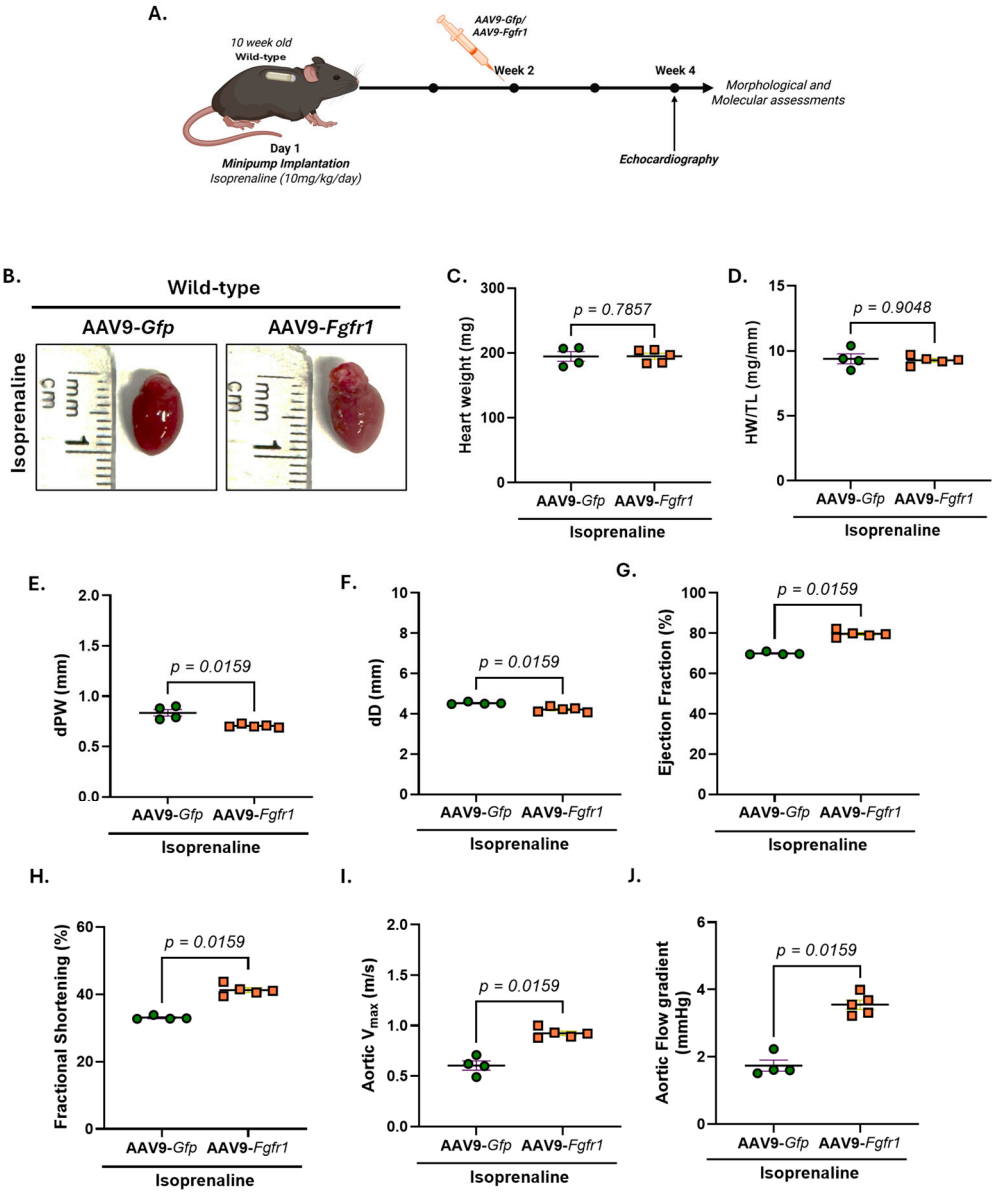


Figure 6. AAV9-mediated FGFR1 re-expression improves ventricular geometry and systolic function under chronic isoprenaline stress. (**A**) Schematic of the experimental design illustrating a 4-week isoprenaline infusion in wild-type (WT) mice followed by a single tail vein injection of AAV9-*Fgfr1* (1×10^{11} viral particles) after 2 weeks of isoprenaline stress. AAV9-*Gfp* (1×10^{11} viral particles)

were injected as controls. Echocardiographic assessment was done after 4 weeks of isoprenaline infusion (2 weeks after AAV9 injection). (**B**) Representative images of excised hearts from isoprenaline-treated WT mice with or without AAV9-*Fgfr1* treatment (ruler shown, 1 cm). (**C**,**D**) Quantification of (**C**) heart weight (HW) and (**D**) HW/tibia length (HW/TL) ratios in hearts receiving FGFR1 overexpression under isoprenaline administration (n = 4–5 hearts/group). (**E**–**J**) Functional echocardiographic parameters in male WT littermates following AAV9-*Fgfr1* treatment under isoprenaline administration. (**E**) Posterior wall thickness in diastole (dPW), (**F**) left ventricular internal diameter in diastole (dD), (**G**) percentage of left ventricular ejection fraction, (**H**) percentage of left ventricular fractional shortening, (**I**) aortic maximal velocity (V_{max}), and (**J**) aortic flow gradient. (n = 4–5 mice/group). Data are presented as mean ± SEM. Statistical significance (p values shown in the panel) was assessed using the Mann–Whitney U test (**C**–**J**).

Importantly, FGFR1 restoration improved cardiac performance. Both ejection fraction and fractional shortening were significantly improved with FGFR1 overexpression (Figure 6G,H; Table S2B). Moreover, both aortic maximal velocity and aortic flow gradient were significantly increased in AAV9-Fgfr1-treated mice under isoprenaline stress (Figure 6I,J; Table S2B), suggesting improved systolic ejection. Together, these data support that restoration of FGFR1 in cardiomyocytes improves cardiac performance during chronic β-adrenergic stress.

3.7. FGFR1 Restoration Alleviates Pathological Remodeling Under Chronic Isoprenaline Stress

To further characterize the functional improvement induced by FGFR1, molecular and histological analyses were performed in WT hearts receiving FGFR1 overexpression under prolonged isoprenaline stress. Immunoblot analyses confirmed a significant increase in AKT phosphorylation under isoprenaline stress against AAV9-*gfp* (Figure 7A,B), demonstrating reactivation of FGFR1-dependent cardioprotective AKT signaling. Analyses of cardiomyocyte CSA revealed no significant difference between AAV9-*Fgfr1* and control groups (Figure 7C,D), reinforcing that FGFR1-mediated rescue occurs independently of changes in single-cell hypertrophy. On the other hand, interstitial and perivascular fibrotic remodeling were markedly attenuated by FGFR1 re-establishment (Figure 7E,F). Additionally, TUNEL staining revealed fewer apoptotic cardiomyocytes following FGFR1 overexpression under chronic isoprenaline infusion (Figure 7G,H). Furthermore, the levels of pathological remodeling marker transcripts, including *Nppb*, *Col3a1*, and *Tgfb1*, were significantly lower in the hearts under isoprenaline stress due to FGFR1 restoration (Figure 7I). Together, these findings demonstrate that FGFR1 overexpression restores AKT signaling and attenuates maladaptive remodeling under persistent isoprenaline-induced β-adrenergic stress.

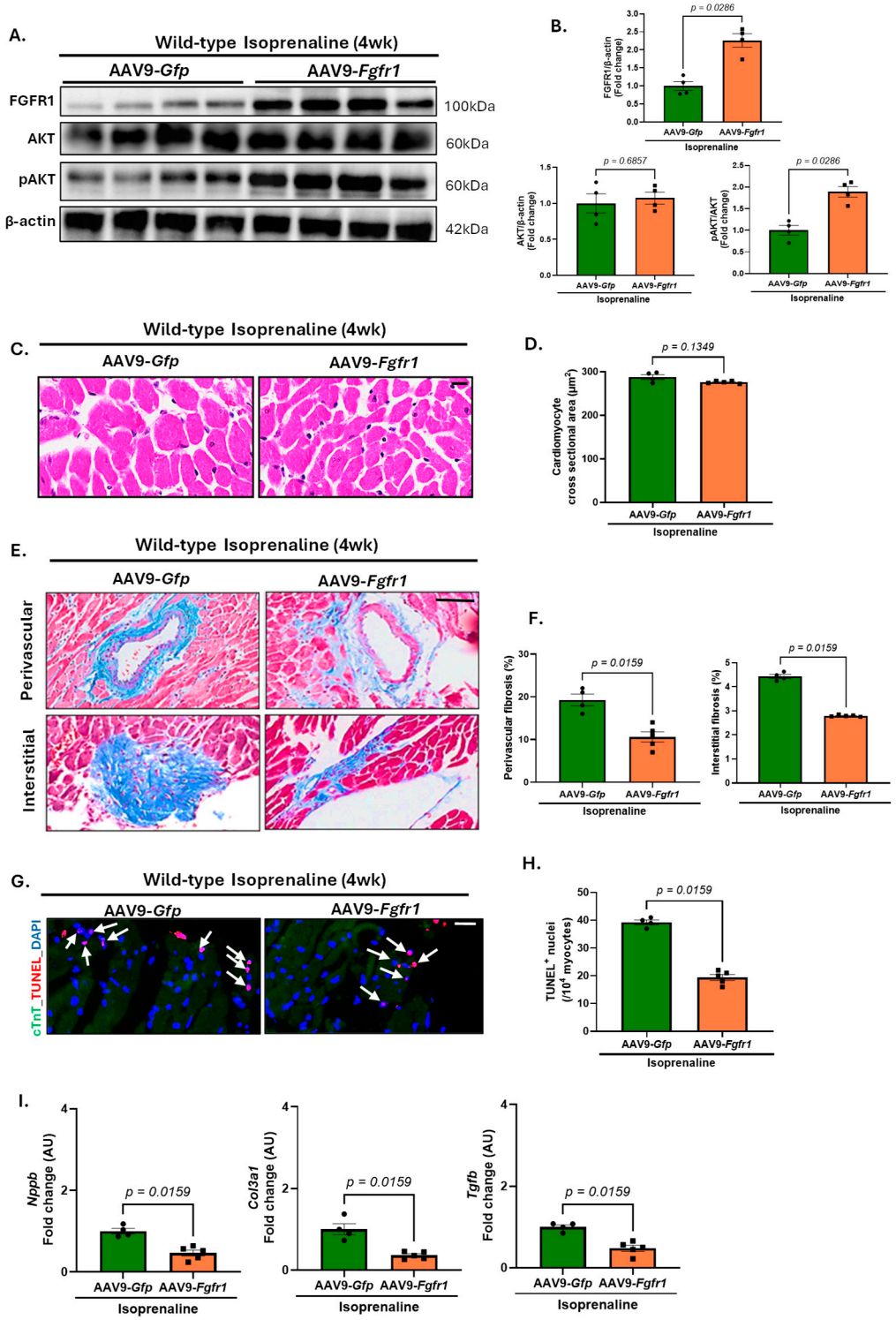


Figure 7. FGFR1 re-expression activates AKT signaling and attenuates maladaptive remodeling. (**A**,**B**) Representative immunoblots and quantification of phosphorylated AKT (pAKT Ser473) and total AKT expression in wild-type (WT) hearts following AAV9-*Fgfr1* treatment under isoprenaline stress (n = 4 hearts/group). Beta actin (β-actin) was used as the loading control. pAKT/AKT ratios normalized to β-actin are shown. (**C**–**H**) Histological assessments of left ventricular tissue in WT hearts following FGFR1 overexpression under isoprenaline stress. (**C**,**D**) Representative H&E-stained cardiac cross-sections and corresponding quantification of cross-sectional area (scale = 20 μm), (**E**,**F**) Representative Masson's Trichrome-stained heart sections showing perivascular and interstitial fibrosis along with quantification (scale = 50 μm), and (**G**,**H**) TUNEL-stained heart sections showing TUNEL-positive nuclei (red; white arrows) along with quantification graph. DAPI is

shown in blue, and green represents cardiac troponin T (cTnT). (n = 4–5 hearts/group, scale = 10 μm). (**I**) Quantitative PCR analysis of *Nppb*, *Col3a1*, and *Tgfb1* transcripts in mouse hearts (n = 4–5 hearts/group). Data are presented as mean ± SEM. Statistical comparisons (indicated in each panel) were performed versus corresponding controls using the Mann–Whitney U test (**B**,**D**,**F**,**H**,**I**).

4. Discussion

The present study identifies FGFR1 as a cardioprotective regulator that facilitates cardiac stress adaptation at least partly through AKT signaling under isoprenaline-induced stress. Cardiomyocyte-specific deletion of FGFR1 exacerbated adverse cardiac remodeling during adrenergic stimulation. In contrast, therapeutic restoration of FGFR1 signaling via AAV9-mediated cardiomyocyte-targeted gene delivery attenuated pathological remodeling and improved cardiac performance even under chronic adrenergic stress, supporting a causal and therapeutically relevant role for FGFR1 in HF progression. Mechanistically, we demonstrated that FGFR1 positively regulates AKT activation, and pharmacological activation of AKT rescued cellular dysfunction induced by FGFR1 deficiency, confirming AKT as a likely key downstream effector of FGFR1-mediated cardioprotection (Figure 8). Collectively, these findings establish FGFR1 as a previously underappreciated regulator of cardiac stress adaptation and identify the FGFR1-AKT signaling axis as a promising therapeutic target for limiting adverse remodeling in HF.

HF remains a major clinical challenge, characterized by progressive ventricular remodeling, chamber dilation, impaired contractile function, and a gradual loss of cardiomyocyte viability. These pathological changes continue to persist despite advances in neurohormonal blockade and device-based therapies, leaving many patients at high risk of morbidity and mortality [3,4]. Consequently, the identification of novel molecular mechanisms and therapeutic strategies capable of counteracting maladaptive remodeling remains a critical unmet need.

In the present study, we utilized human myocardial tissue to identify dysregulated signaling pathways directly relevant to clinical disease. Integrated proteomic and transcriptomic analyses revealed broad disruption of remodeling-associated pathways in HF, with prominent suppression of AKT signaling. Prior analyses of failing human myocardium have reported reduced AKT phosphorylation in the skeletal muscle compared with healthy controls [23]. Furthermore, other studies have reported reduced phosphorylation of AKT1 during congestive cardiomyopathy [24]. Although our dataset did not assess individual AKT isoforms, the observed suppression of AKT signaling is consistent with prior reports, supporting the concept that loss of cardioprotective AKT activity represents a feature of advanced HF.

AKT plays a complex, context-dependent role in the heart, acting as a central regulator of cardiomyocyte survival, metabolism, and adaptive growth. Under physiological conditions, growth factors such as insulin and insulin growth factor-1 (IGF-1), as well as exercise, activate AKT signaling through the phosphoinositide 3-kinase (PI3K) pathway [25]. Activation of receptor tyrosine kinases, including FGFR1, leads to recruitment of adaptor proteins such as fibroblast growth factor receptor substrate 2 (FRS2) and growth factor receptor-bound protein 2 (GRB2), which stimulate PI3K activity to recruit AKT to the plasma membrane [26], where it undergoes phosphorylation at Thr308 by 3-phosphoinositide-dependent kinase-1 (PDK1) and at Ser473 by mechanistic target of mTORC2 [25]. However, the reaction is likely blocked by loss of SIN1, which is the core structural regulatory subunit for mTORC2 and can facilitate the phosphorylation of AKT at Ser437 [22]. In contrast, reduced growth factor signaling or physical inactivity is associated with diminished phosphorylation at these regulatory residues and consequent attenuation of AKT activity [25]. This mechanism may explain the reduction in AKT phosphorylation observed in FGFR1-deficient hearts. However, the specific downstream signaling events

linking FGFR1 activation to AKT regulation in cardiomyocytes under β-adrenergic stress were not directly investigated in the present study and warrant further mechanistic investigation in the future.

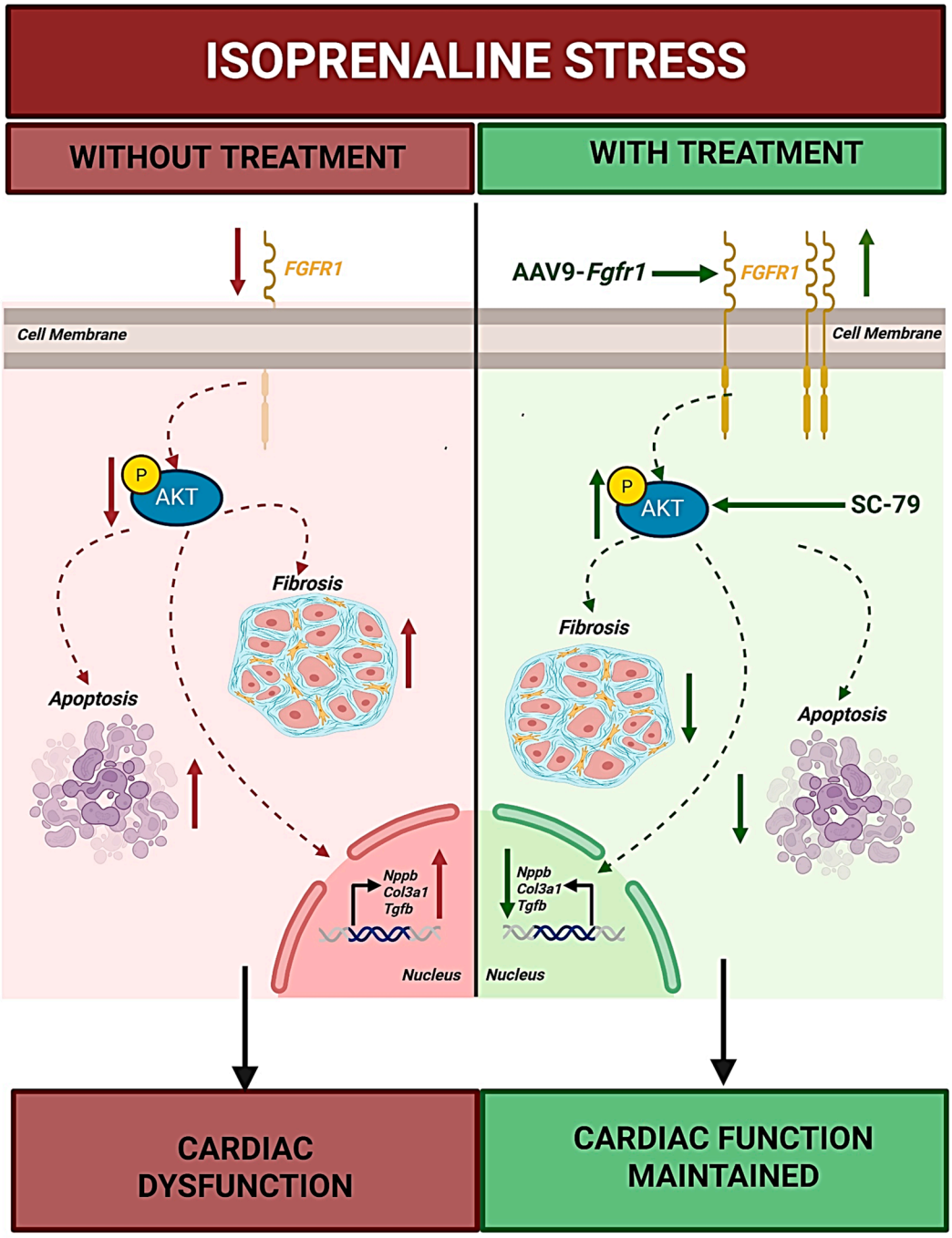


Figure 8. Schematic illustrating FGFR1-AKT signaling regulating cardiac remodeling under isoprenaline stress. Isoprenaline stress suppresses FGFR1 expression, leading to reduced AKT phosphorylation and activation. This results in enhanced fibrosis and apoptosis, leading to progressive deterioration of cardiac systolic function. In contrast, genetic restoration of FGFR1 expression by AAV9-*Fgfr1* treatment or pharmacological activation of AKT with SC-79 re-establishes AKT signaling, limits maladaptive remodeling, and preserves cardiac function under isoprenaline stimulation. Red arrows indicate upregulation. Green arrows indicate downregulation.

Functionally, phosphorylation at Thr308 is required for catalytic activation of AKT kinase activity, whereas phosphorylation at Ser473 stabilizes the active conformation of

the kinase and enhances signaling efficiency [27]. Accumulating evidence suggests that Ser473 phosphorylation may play a particularly important role in regulating stress-responsive AKT signaling in the heart, including pathways governing cardiomyocyte survival and metabolic adaptation during cardiac injury and HF [25,28–31]. Therefore, in the present study, we evaluated AKT activation primarily through phosphorylation at Ser473, which is widely used as a marker of AKT pathway activity in cardiac stress models [10,30,32]. Although Thr308 phosphorylation was not assessed, future studies examining both regulatory sites will be necessary to determine whether differential regulation of AKT phosphorylation contributes to signaling alterations during β-adrenergic stress-induced HF.

Prompted by the protective roles of FGFR1 in endothelial cells [32] and in models of diabetes [12], and acute ischemia–reperfusion injury (I/R) [15], we sought to examine its function under chronic β-adrenergic stress using a cardiomyocyte-specific conditional knockout model subjected to isoprenaline. Previous studies provide evidence supporting a functional connection between FGF-FGFR signaling and AKT-mediated cardio-protection in other models. For example, studies in zebrafish have demonstrated that FGFR1 signaling activates AKT to support cardiomyocyte survival and cardiac regeneration following injury [33]. In mammalian models of ischemia–reperfusion injury, cardiomyocyte-specific deletion of both FGFR1 and FGFR2 exacerbates pathological remodeling and worsens cardiac function after reperfusion [15], highlighting the importance of FGFR signaling in myocardial repair and stress adaptation.

Our findings extend previous studies, demonstrating that cardiomyocyte FGFR1 regulates AKT activation during chronic β-adrenergic stress. Loss of FGFR1 resulted in reduced AKT signaling accompanied by impaired cardiac function, increased apoptosis, and enhanced fibrosis. Importantly, pharmacological activation of AKT using SC-79 rescued the cellular dysfunction induced by FGFR1 deficiency, suggesting that the detrimental effects of FGFR1 loss are mediated through suppression of AKT signaling. Together, these findings support a model in which FGFR1 maintains cardiomyocyte homeostasis, at least partly, by promoting AKT-dependent survival signaling during β-adrenergic stress.

Previous studies have shown that the inactivation of FGFR1 and FGFR2 in cardiomyocytes in mice exhibits exacerbated ventricular remodeling seven days post ischemia–reperfusion injury, characterized by increased pathological remodeling despite no significant change in cardiomyocyte size in the remote myocardium [15]. Similarly, in our model, FGFR1-deficient hearts displayed cardiomyocyte growth comparable to controls under isoprenaline-induced adrenergic stress, yet showed markedly increased fibrosis and apoptosis, indicating a dissociation between hypertrophic growth and maladaptive remodeling. Consistent with this observation, the worsened phenotype in FGFR1-deficient hearts occurred despite preserved cardiomyocyte cross-sectional area, suggesting that impaired systolic performance was not driven by alterations in single-cell hypertrophy. This finding aligns with previous studies demonstrating that cardiac dysfunction can develop independently of cardiomyocyte size, instead reflecting changes in myocardial architecture, cardiomyocyte survival, and extracellular matrix remodeling [34–36]. Collectively, these findings suggest that cardiomyocyte FGFR1 plays a critical role in coordinating adaptive stress responses in the heart, particularly by limiting fibrosis and cardiomyocyte loss. Disruption of FGFR1 signaling therefore promotes maladaptive remodeling and accelerates the transition toward decompensated HF.

Consistent with the proposed FGFR1-AKT signaling axis, cardiomyocyte-specific loss of FGFR1 resulted in reduced AKT activation, without affecting cardiomyocyte hypertrophy. Importantly, activation of AKT signaling through cardiomyocyte-specific overexpression of FGFR1 attenuated cardiac dysfunction and maladaptive remodeling

without further increasing cardiomyocyte size. These findings indicate that enhancement of AKT upstream signaling during chronic β-adrenergic stress can restore cardioprotective pathways without promoting excessive hypertrophic growth.

Previous studies have demonstrated that moderate or transient activation of AKT enhances cardiomyocyte survival and improves cardiac function under pressure overload [37] or ischemic stress [28], whereas sustained or constitutive AKT activation in transgenic mice can drive pathological hypertrophy [6,38,39]. In contrast to direct AKT overexpression, FGFR1 overexpression in our model appears to restore AKT signaling toward physiological levels rather than amplifying it beyond normal thresholds. Supporting this interpretation, pharmacological activation of AKT using SC-79 also improved FGFR1-loss-induced cellular dysfunction without further inducing hypertrophic changes. We next asked whether an intact FGFR1 activates AKT through mTORC2 in cardiomyocytes. We found that FGFR1 overexpression-enhanced AKT phosphorylation was blocked by SIN1 deficiency, supporting that FGFR1 likely depends on AKT through mTORC2 to alleviate isoprenaline complications. However, whether and how FGFR1 activates mTORC2 was not studied in the present work. Together, these findings suggest that FGFR1-mediated physiological AKT signaling could preserve cardiac function and attenuate pathological remodeling without promoting unnecessary maladaptive hypertrophy associated with excessive AKT overactivation, highlighting the FGFR1-AKT axis as a potentially attractive therapeutic target from a translational perspective.

This study has several limitations. First, the evidence linking FGFR1 to AKT signaling is based on in vitro experiments and does not establish that FGFR1 mediates AKT signaling in vivo. Animal studies and further functional validation are needed to clarify the mechanisms and clinical translational implications. Second, the human sample size was limited, and although the samples were from patients with HF, their underlying diseases and comorbidities varied. The observed changes in FGFR1/AKT signaling should therefore be interpreted as associations with HF, rather than evidence that this pathway is a specific or sole cause. Finally, the present results support AKT as one pathway regulated by FGFR1, but do not exclude contributions from other FGFR1-mediated signaling pathways in cardiomyocytes.

5. Conclusions

In summary, FGFR1 functions as a likely positive regulator of AKT-dependent cardioprotective signaling in HF. Its loss is a causative factor in inducing cardiac maladaptive remodeling and functional decline, whereas genetic restoration of FGFR1 maintains physiological activation of AKT, eliciting therapeutic effects on HF under pathological stress. These results highlight FGFR1 as a potential target for the treatment of HF.

Supplementary Materials: The following supporting information can be downloaded at https://www.mdpi.com/article/10.3390/biom16111621/s1, Figure S1: Validation of FGFR1 cardiac knockout; Figure S2: Validation of FGFR1 knockdown in H9C2 cells; Figure S3: FGFR1 levels are reduced after prolonged isoprenaline stress in neonatal rat cardiomyocytes (NRCMs); Table S1: Morphometric and Echocardiographic assessment of male FGFR1Flox and FGFR1cKO mice after 2 weeks of isoprenaline stress; Table S2: Morphometric and Echocardiographic assessment of male wild-type under isoprenaline stress, followed by AAV9-Gfp or AAV9-Fgfr1 treatment. File S1: Original Western blot images for Figures 1, 3–5, 7 and S1–S3.

Author Contributions: W.L. conceived and supervised the study. N.H.A. and S.R.G. led experimental design, execution, data collection and analyses, and manuscript drafting. N.H.A., Y.H., and M.F. carried out manuscript review and proofreading. O.F., J.Z. and X.C. contributed to manuscript drafting. Y.H. and W.L. performed neonatal rat cardiomyocyte isolations and culture. W.L. also

performed osmotic minipump implantation surgeries and echocardiographic assessments. Human heart tissue samples were provided by R.R.E.A. and T.M.A.M. T.W. and S.A. contributed strategic guidance and mentorship, and E.J.C. provided critical evaluation of the in vivo work. B.D.K., supported by a British Heart Foundation Personal Chair, also provided financial support for the work. All authors have read and agreed to the published version of the manuscript.

Funding: This work was mainly supported by the British Heart Foundation (FS/19/70/34650, PG/19/66/34600, FS/PhD/22/29307, PG/22/10904, PG/22/11075, and PG/24/12025 to W.L; BHF Accelerator award AA/18/4/34221 to the University of Manchester); and Manchester FBMH Doctoral Academy Studentship to S.R.G., B.D.K. was supported by a BHF Personal chair (CH/13/2/30154). T.M.A.M. is supported by NIH grants R01HL147921 and P30GM127607, U.S.A. Department of Defense grant W81XWH-20-1-0419, and American Heart Association grant 16SDG29950012. The authors also acknowledge NIH grant F32HL149140 (R.R.E.A.).

Institutional Review Board Statement: Human hearts were obtained from two sources. Samples purchased from Asterand (BioIVT; sale ID 224622, 19/04/2021) were collected with ethical approval in accordance with United Kingdom Human Tissue Authority regulations. Samples from de-identified donors obtained through the United Network for Organ Sharing (UNOS) were determined to be non-human subject research by the Institutional Review Board of Baylor College of Medicine (protocol H-53940, 30/06/2023). The animal study protocol was approved by the University of Manchester Ethics Committee under the PPL license PP0172073 (23/09/2025) and PA8E7CA4E (29/09/2020).

Informed Consent Statement: Informed consent for research use of the Asterand (BioIVT) samples was obtained by the supplier in accordance with United Kingdom Human Tissue Authority regulations. UNOS samples were obtained from de-identified donors.

Data Availability Statement: The RNA-sequencing data have been deposited in ArrayExpress under accession number E-MTAB-16575. The mass spectrometry proteomics data have been deposited in the ProteomeXchange Consortium via the PRIDE partner repository with the dataset identifier PXD086105. Other data supporting the findings of this study are available from the corresponding author upon reasonable request.

Acknowledgments: The authors gratefully acknowledge the support of staff across multiple departments at The University of Manchester, whose expertise and assistance were invaluable to this project. We sincerely thank Steven Marsden, Peter March, and James Bagnall from the Bioimaging Facility for their training and technical support in fluorescence microscopy. We also acknowledge Bharatkumar Rash, Andy Hayes, Ian Donaldson, Rachel Scholey, and Leo Zeff from the Genomic Technologies and Bioinformatics Facilities for assistance with RNA sequencing and data analysis. We also thank Stacey Warwood, James Allsey, Melissa Kidd, Julian Selley, and David Knight from the Mass Spectrometry Facility for expert advice and support with sample preparation, proteomic analysis, and data interpretation. Finally, we thank Charlotte Beck and Victoria Perks from the Biological Services Facility for their guidance in animal training, handling, and husbandry.

Conflicts of Interest: T.M.A.M. holds equities at Tenaya Therapeutics. All other authors have declared that no conflict of interest exists.

Appendix A. Supplemental Methods

Appendix A.1. Animal Studies

All animal studies were performed in accordance with the United Kingdom Animals (Scientific Procedures) Act 1986 and were approved by the University of Manchester Ethics Committee under the PPL license PP0172073 (23/09/2025) and PA8E7CA4E (29/09/2020). All mice and rats were housed in conventional conditions in an animal facility at the University of Manchester with food and water provided ad libitum in a 12 h

light/dark cycle. The animals were euthanized in accordance with directive 2010/63/EU of the European Parliament and in compliance with the ethical standards of the University of Manchester and the UK Home Office Animals (Scientific Procedures) Act 1986. This study utilized FGFR1 cardiomyocyte-specific knockout mice ($FGFR1^{cko}$). Fibroblast growth factor 1 (*Fgfr1*) floxed mice ($FGFR1^{fl/+}$) were purchased from Jackson laboratory (B6.129S4-Fgfr1tm5.1Sor/J, RRID: IMSR_JAX:007671) and mated with transgenic mice expressing Cre under α myosin heavy chain (αMHC) promoter to generate cardiomyocyte-specific *Fgfr1* knockout mice ($FGFR1^{cKO}$). Floxed littermates ($FGFR1^{Flox}$) were used as controls. Once weaned, 10-week-old male mice were used for experiments. Cohort sizes were estimated based on a preliminary study using >80% power, $\alpha = 0.05$. Aside from strain, age and sex, no exclusion/inclusion criteria were set, and all animals are presented in the data. Animals were randomly allocated into groups using an online random group generator, and investigators were blinded to experimental groups for data analysis.

Appendix A.2. Human Samples

Human hearts were either purchased from Asterand (BioIVT, Bioivt.com, sale ID 224622, 19/04/2021; Asterand obtained ethical approval and consent following the United Kingdom Human Tissue Authority regulations) or obtained from the transplantation network in the USA (UNOS) from de-identified donors and we have obtained approval from the Institutional Review Board of Baylor College of Medicine for non-human subject research (protocol number H-53940 (30/06/2023). Heart tissue samples were collected from patients with heart failure (HF) and from non-failing control donors. Tissue samples were used for RNA sequencing and Mass spectrometry followed by pathway enrichment analysis. All experimental procedures performed on human samples were approved by the University of Manchester Research Ethics Committees and in agreement with the Declaration of Helsinki (12172, the Human Tissue Authority, 18/09/2020). The following inclusion and exclusion criteria were applied.

Non-failing control donors:

- Inclusion criteria included: left ventricular ejection fraction (LVEF) > 55%.
- Exclusion criteria included: (1) history of myocardial infarction, (2) pregnancy, (3) decompensated heart failure, (4) severe kidney disease, (5) asthma or severe chronic lung disease, (6) presence of a cardiac pacemaker or implantable defibrillator, (7) cerebral aneurysm clip, (8) neural stimulator, and (9) history of diabetes.

HF donors:

- Inclusion criteria were (1) LVEF < 40%, (2) presence of at least one of the following comorbidities: myocardial infarction, congestive heart failure, hypertension, coronary artery disease, or diabetes.
- Exclusion criteria included: (1) pregnancy, (2) asthma or severe chronic lung disease, (3) cerebral aneurysm clip, and (4) neural stimulator.

Detailed demographic characteristics of the donors are provided in Table A1 below.

Table A1. Detailed demographic characteristics of human sample donors.

Heart	Age	Gender	Ethnicity	Comorbidities
Control (For Mass spectrometry)				
1	51	Male	Hispanic/Latino	None
2	61	Male	Caucasian	None
3	61	Female	Caucasian	None
4	56	Female	Caucasian	None
5	51	Female	Caucasian	None
6	61	Male	African American	None
7	61	Female	Caucasian	None

8	68	Male	Caucasian	None
Heart failure (HF) (For Mass spectrometry)				
1	48	Female	Caucasian	Myocardial infarction
2	39	Male	Hispanic/Latino	Myocardial infarction, Hypertension
3	62	Male	Not reported	Congestive heart failure, Myocardial infarction
4	65	Male	Caucasian	Congestive heart failure, Hypertension
5	63	Male	Caucasian	Coronary artery disease, Chest trauma, Hypertension
6	64	Male	Caucasian	Coronary artery disease, Chest trauma, Hypertension, Aortic graft, Stent placed for myocardial infarction
7	74	Male	Not reported	Coronary artery disease
Control (For RNA sequencing)				
1	46	Female	Black or African American	Hypothyroidism
2	58	Female	Native American or Alaskan Native	None
3	44	Male	Caucasian	None
4	44	Male	Caucasian	None
Heart failure (HF) (For RNA sequencing)				
1	48	Female	Caucasian	Myocardial infarction
2	39	Male	Hispanic/Latino	Hypertension, Myocardial infarction
3	62	Male	Not reported	Congestive heart failure, Myocardial infarction
4	65	Male	Caucasian	Congestive heart failure, Hypertension
5	57	Male	African American	Restrictive cardiomyopathy, Hypertension
6	57	Female	African American	Hypertension, Type II diabetes, Neuropathy

Appendix A.3. Isoprenaline-Induced Stress

Cardiac β-adrenergic stress was induced by administration of isoprenaline (I6504, Sigma-Aldrich) for 2–4 weeks at 10 mg/kg/day via osmotic mini-pumps (Charles River, 2004) implantation, as described previously [16]. Briefly, the subcutaneous Alzet minipump was implanted in the lower dorsal area for continuous delivery of isoprenaline in 10-week-old $FGFR1^{Flox}$ or $FGFR1^{cKO}$ male mice. Control mice received an Alzet minipump containing 0.9% saline solution. Mice were anesthetized with 2.5% isoflurane inhalation. Analgesia was provided by a subcutaneous injection of 0.1 mg/kg buprenorphine. The study continued for 2–4 weeks as highlighted in the results.

Appendix A.4. Adeno-Associated Virus 9 (AAV9) FGFR1 Treatment

Cardiac-specific FGFR1 overexpression was achieved using an adeno-associated virus serotype 9 (AAV9) vector carrying mouse *Fgfr1* cDNA (VectorBuilder) under the control of the cardiac troponin T (cTnT) promoter. Viral packaging of AAV9-cTnT-m*Fgfr1*-Myc was performed by Boston Children's Hospital. FGFR1 overexpression was induced by tail vein injection of AAV9-*Fgfr1* at a dose of 1×10^{11} viral particles per mouse in 10-week-old $FGFR1^{Flox}$ mice, following two weeks of isoprenaline delivery via osmotic minipump implantation. Mice injected with an AAV9 vector encoding enhanced GFP under the cTnT promoter (AAV9-cTnT-e*Gfp*) served as controls and were administered the same number of viral particles.

Appendix A.5. Echocardiography

Transthoracic echocardiography was performed using the Acuson Sequoia C256 (Siemens) system. Two-dimensional (2D), M-mode, and pulse-wave Doppler images were acquired in anesthetized mice. Animals were sedated with 2% isoflurane delivered in 100% oxygen at a flow rate of 1.5 L/min throughout the procedure. Left ventricular (LV) chamber dimensions and wall thicknesses were obtained from M-mode images, including

diastolic posterior wall thickness (dPW). Systolic function was assessed by calculating fractional shortening and ejection fraction. Pulse-wave Doppler recordings were used to evaluate LV outflow parameters, including maximum aortic velocity (aortic V_{max}) and the corresponding aortic flow pressure gradient. Additional echocardiographic parameters and group comparisons are summarized in the Supplemental Tables.

Appendix A.6. Embedding and Sectioning of Heart Tissue

Freshly excised hearts were weighed to determine heart weight (HW). Cardiac hypertrophy was assessed by normalizing heart weight to tibia length (HW/TL). Hearts were then transversely sectioned, fixed overnight in 4% paraformaldehyde (PFA), and embedded in paraffin wax for histological analysis. Serial sections (5 μm thick) were cut using Leica RM2135 microtome.

Appendix A.7. Hematoxylin and Eosin (H&E) Staining

Hematoxylin and eosin (H&E) staining was performed on myocardial paraffin sections to assess cardiomyocyte cross-sectional areas in response to isoprenaline stress. Sections were deparaffinized and rehydrated, then stained with Harris' hematoxylin (Sigma-Aldrich, HHS32) for 5 min and differentiated in acid alcohol [1% (*v*/*v*) hydrochloric acid in 70% ethanol] for 10 s. Sections were subsequently counterstained with eosin (ThermoFisher Scientific, 6766007) for 1 min. Slides were dehydrated through three changes of 100% industrial methylated spirits (IMS), cleared in xylene, and mounted using a xylene-based mounting medium (Eukitt, Sigma-Aldrich).

Appendix A.8. Masson's Trichrome Staining

Masson's trichrome staining was performed on myocardial paraffin sections to assess interstitial and perivascular fibrosis in response to isoprenaline stress. Sections were deparaffinized and rehydrated, then immersed in Bouin's solution (Sigma-Aldrich, HT10132) for 2 h. Nuclei were stained with Harris' hematoxylin for 5 min and differentiated in acid alcohol for 10 s. Cardiomyocytes were subsequently stained with Biebrich scarlet-acid fuchsin (Sigma-Aldrich, HT151), followed by collagen staining with aniline blue (Sigma-Aldrich, B8563). Sections were then dehydrated by IMS, cleared in xylene, and mounted using a xylene-based mounting medium (Eukitt, Sigma-Aldrich).

Appendix A.9. TdT-Mediated dUTP Nick-End Labelling (TUNEL) Assay

Apoptotic cells in myocardial tissue sections were detected using a terminal deoxynucleotidyl transferase-mediated dUTP nick-end labeling (TUNEL) assay (Roche, 11684795910), performed according to the manufacturer's instructions. Co-staining with anti-cardiac troponin T antibody (ProteinTech, 15513-1-AP) was performed to detect cardiomyocytes. Following staining, sections were mounted with ProLong™ Gold Antifade Mountant containing DAPI (ThermoFisher Scientific, P36935).

Appendix A.10. Real-Time Quantitative Polymerase Chain Reaction (RT-qPCR)

Total RNA was extracted utilizing Trizol and treated with DNAse (Invitrogen, AM1906) to eliminate genomic DNA contamination. Total RNA was converted into complementary DNA (cDNA) using LunaScript (New England Biolabs, E3010) as described by the manufacturer. The qPCR reaction was achieved via 30 ng cDNA using SYBR Select PCR master mix (Applied Biosystems, 4472908), followed by running on the Applied Biosystems QuantStudio™ Flex System. The fold change was measured using the comparative threshold (Ct) method (CT method) [40]. Target gene expression was normalized to *18S* ribosomal RNA for mouse and rat samples.

Appendix A.11. RNA Sequencing

Total RNA from control and failing hearts were extracted using Trizol and treated with DNAse as mentioned above. RNA quality and integrity were evaluated using an Agilent 2100 Bioanalyzer. mRNA libraries were generated using the TruSeq Stranded mRNA assay (Illumina), employing poly(A)-based enrichment of mRNA with concurrent removal of rRNA, as previously described [41]. The altered genes ($p < 0.05$ in HF samples versus control non-failing samples) were selected for pathway analyses using Enrichr (https://maayanlab.cloud/Enrichr/, 22 October 2026) or ShinyGo v0.82 (https://bioinformatics.sdstate.edu/go82, 22 October 2026). The *p* values are calculated using the Wald test, while multiple testing correction of adjusted *p* (*Padj*.) values was performed by Benjamini–Hochberg method. Significantly altered pathways (*Padj.* < 0.05 Reactome) were used to generate the pathway enrichment dot plots using SRPlot [42], focusing on Gene Ontology (GO) pathways and associated biological processes.

Appendix A.12. Liquid Chromatography–Tandem Mass Spectrometry (LC-MS/MS)

To determine changes in protein expression in human failing hearts, protein profiling was performed via LC-MS/MS as previously described [12] . The proteins were annotated according to the SwissProt protein database with false discovery rates set to 1%. The differential expression results were analyzed using Spectronaut (Biognosys), using Bonferroni correction. Differentially expressed proteins ($p < 0.05$ in HF hearts compared to control hearts) were selected and analyzed using Enrichr (https://maayanlab.cloud/Enrichr/, 22 October 2026) or ShinyGo v0.82 (https://bioinformatics.sdstate.edu/go82, 22 October 2026). Altered pathways ($p < 0.05$ Reactome) were used to generate the pathway enrichment dot plots using SRPlot, focusing on Gene Ontology (GO) pathways and associated biological processes. [42].

Appendix A.13. Neonatal Rat Cardiomyocytes (NRCMs)

Neonatal rat cardiomyocytes were isolated from 2/3-day-old male and female Sprague–Dawley rats, as described previously [41]. Briefly, extracted hearts were dissected into small pieces and subjected to consecutive cycles of enzymatic digestion, for 7 min/cycle, in 7 mL of buffer [116 mM NaCl, 20 mM, 1 mM NaH_2PO_4, 6 mM glucose, 5 mM KCl, 0.8 mM $MgSO_4$, pH 7.4] containing 0.33 U/mL Collagenase A (Roche, 10103586001) and 100 mg/mL pancreatin (Sigma-Aldrich, P3292). Cardiomyocytes were then cultured in maintenance medium [80% DMEM, 20% M199, 1% FBS, penicillin-streptomycin, fungizone, and 1 M bromodeoxyuridine] prior to treatments.

Appendix A.14. H9C2 Cell Culture

H9C2 rat myoblasts (Sigma-Aldrich, 88092904) were maintained in DMEM (Gibco, 11966) supplemented with 10% (*v*/*v*) heat-inactivated fetal bovine serum (FBS), 100 μg/mL streptomycin, and 100 U/mL penicillin.

Appendix A.15. Isoprenaline Stimulation In Vitro

To mimic isoprenaline-induced myocardial injury in vivo, an in vitro model was established using NRCMs and H9C2 cells. Briefly, when cells reached approximately 80% confluence, the culture medium was removed, and the cells were treated with isoproterenol (10 μM; Sigma-Aldrich, I6504) for 8 h in DMEM containing 10% (*v*/*v*) heat inactivated FBS, 100 μg/mL streptomycin, and 100 U/mL penicillin. This dose was chosen based on prior experiments [43].

Appendix A.16. siRNA Knockdown of FGFR1 and SIN1

FGFR1 knockdown in vitro was accomplished utilizing Lipofectamine LTX & Plus Reagent (ThermoFisher Scientific, 15338-100) mediated transfection of Silencer Select Pre-Designed rat si*Fgfr1* (S135014, ThermoFisher Scientific) and Silencer Select PreDesigned rat si*SIN1*/si*MAPKAP1* (S150327, ThermoFisher Scientific), following the instructions of the manufacturer. The control cells were transfected with a negative control si*RNA* (si*Negative*). Cells transfected with 50 nM of siRNA were incubated for 48 h at 37 °C before further treatment.

Appendix A.17. FGFR1 Overexpression

FGFR1 were overexpressed in cells by infection with Adv-*Fgfr1* (VectorBuilder, adenovirus overexpressing FGFR1), at a multiplicity of infection (MOI) of 50.

Appendix A.18. SC-79 Treatment

10 μM of SC-79 (MedChemExpress, HY-18749) was utilized to activate AKT pathway. NRCMs and H9C2 cells were treated with SC-79 for 8 h together with isoprenaline stimulation. This dose was selected based on the previous literature [10].

Appendix A.19. Immunocytofluorescence Staining

Immunofluorescence staining was executed on NRCMs and H9C2 cells following treatment as stipulated in the results. Cells were fixed and permeabilized with cold methanol at 4 °C for 20 min. Subsequently, coverslips were blocked with 1% (*w*/*v*) BSA in PBS, followed by incubation with α-actinin antibody conjugated with AlexaFluor 488 fluorescent-conjugated (1:100; Proteintech, CL488-11313) diluted in 0.5% (*w*/*v*) BSA in PBS overnight. Finally, the coverslips were washed with 0.5% (*w*/*v*) BSA in PBS, to reduce non-specific binding and background signal, then mounted with ProLong™ Gold Antifade Mountant containing DAPI (ThermoFisher Scientific, P36935).

Appendix A.20. Cell Viability Assay

CellTiter-Glo® Luminescent Cell Viability Assay (Promega, G9241) was performed according to the manufacturer's protocol. Briefly, 25,000 cells/well were plated overnight in an opaque-walled 96-well plate (Corning costar, 3596). NRCMs were treated as described in the results for the indicated period. To measure activity, 100 μL of CellTiter-Glo® 2.0 Reagent was added to each well for 10 min with constant shaking at room temperature. Luminescence was measured using Promega GloMax® Explorer plate reader.

Appendix A.21. Cytotoxicity Assay

Cytotoxicity was measured by CellTox™ Green Cytotoxicity Assay (Promega, G182B). Briefly, 10,000 cells/well were plated overnight in a black-walled 96-well plate (Corning costar, 3603). NRCMs were treated as described in the results for the indicated period. CellTox™ Green reagent was diluted 1:1000 and applied to cells followed by a 15 min dark incubation. Fluorescence was measured at Ex/Em: 475/500–550 nm using a Promega GloMax® Explorer plate reader.

Appendix A.22. Protein Lysates Extraction and Immunoblotting

Cell and tissue total protein lysates were obtained utilizing Triton lysis buffer [20 mM Tris, 137 mM NaCl, 2 mM EDTA, 0.1% (*w*/*v*) SDS, 10% (*v*/*v*) glycerol, 1% (*v*/*v*) Triton-X, 25 mM glycerophosphate, protease and phosphatase inhibitor cocktail, pH 7.4]. Protein concentration was calculated using the Bradford assay (Bio-Rad, 500-0006) and immunoblotting was conducted using 30 μg protein lysate. Primary antibodies [FGFR1 (1:1000; Santa

Cruz Biotechnology, sc-57132), SIN1/MAPKAP1 (1:1000; Proteintech, 15463-1-AP), AKT (1:1000; Proteintech, 60203-2-Ig), pAKT (1:1000; Cell Signaling, 4060S), GAPDH (1:1000; Abcam, 9484), and Beta-actin (β-Actin; 1:1000: Proteintech, 66009-1-IG] along with HRP conjugated secondary antibodies (HRP-linked anti-mouse; 1:2000; Proteintech, RGAM001 and HRP-linked anti-rabbit; 1:1000; Cell Signalling Technology, 7074S) were diluted in 5% (*w*/*v*) fat free milk in TBS-T. Amersham ECL Prime (RPN2232) or Select (RPN2235) detection solutions were used to observe protein bands via chemiluminescent imaging by the ChemiDoc MP system (Bio-Rad).

Appendix A.23. Imaging Histology

H&E- and Masson's-stained heart sections were imaged on a 3D-Histech Pannoramic-250 microscope slidescanner using a Zeiss 20×/0.80 Plan Apochromat objective. Snapshots of the scanned slides were taken using the Case Viewer software (3D-Histech) with individual magnification. Fluorescent-labelled slides for TUNEL and α-actinin staining were imaged using a Zeiss Axioimager D2 upright microscope with Zeiss LD Plan-Neofluar objectives (×20) and captured using a Coolsnap HQ2 camera (Photometrics) through Micromanager software v1.4.23. Specific band pass filter sets for DAPI, FITC, and Texas Red were used to prevent bleeding from one channel to the next. Images were then further processed and analyzed using Image J software (v1.54g).

Appendix A.24. Statistical Analyses

Data are exhibited as bar/dot plots showing mean ± SEM. Shapiro–Wilk test was conducted to evaluate whether data was normally distributed. Normally distributed data sets were analyzed using ordinary One-way or Two-way ANOVA followed by appropriate post hoc tests, whereas assessments between only two groups utilized two-tailed Student's unpaired *t*-test. If the data were not normally distributed, non-parametric tests (equivalent to one-way ANOVA and Student's *t*-test), such as the Kruskal–Wallis test or the Mann–Whitney U test, were used. Statistical analysis was conducted utilizing the GraphPad Prism 10 (v10.2.2) software and p values < 0.05 were considered statistically significant. The sample size corresponds to biological replicates and is specified for each experiment within the figure legend.

References

1. Køber, L.; Adamo, M.; Ruwald, A.-C.; Tomasoni, D.; Anderson, L.J.; Andersson, C.; Brugts, J.J.; Chioncel, O.; Donal, E.; Ferdinandy, P.; et al. 2026 ESC Guidelines for the Management of Heart Failure. *Eur. Heart J.* **2026**, *47*, 5346–5457. https://doi.org/10.1093/eurheartj/ehag100.
2. Savarese, G.; Becher, P.M.; Lund, L.H.; Seferovic, P.; Rosano, G.M.C.; Coats, A.J.S. Global Burden of Heart Failure: A Comprehensive and Updated Review of Epidemiology. *Cardiovasc. Res.* **2023**, *118*, 3272–3287. https://doi.org/10.1093/cvr/cvac013.
3. He, X.; Du, T.; Long, T.; Liao, X.; Dong, Y.; Huang, Z.-P. Signaling Cascades in the Failing Heart and Emerging Therapeutic Strategies. *Signal Transduct. Target. Ther.* **2022**, *7*, 134. https://doi.org/10.1038/s41392-022-00972-6.
4. Vaduganathan, M.; Fonarow, G.C.; Greene, S.J.; DeVore, A.D.; Kavati, A.; Sikirica, S.; Albert, N.M.; Duffy, C.I.; Hill, C.L.; Patterson, J.H.; et al. Contemporary Treatment Patterns and Clinical Outcomes of Comorbid Diabetes Mellitus and HFrEF. *JACC Heart Fail.* **2020**, *8*, 469–480. https://doi.org/10.1016/j.jchf.2019.12.015.
5. Meco, M.; Giustiniano, E.; Nisi, F.; Zulli, P.; Agosteo, E. MAPK, PI3K/Akt Pathways, and GSK-3β Activity in Severe Acute Heart Failure in Intensive Care Patients: An Updated Review. *J. Cardiovasc. Dev. Dis.* **2025**, *12*, 266. https://doi.org/10.3390/jcdd12070266.
6. Khetarpal, S.A.; Li, H.; Lerchenmüller, C.; Rhee, J.; Rosenzweig, A. Molecular Mediators of the Cardiac Benefits of Exercise. *Circ. Res.* **2025**, *137*, 163–183. https://doi.org/10.1161/CIRCRESAHA.125.325762.
7. Song, H.-P.; Chu, Z.-G.; Zhang, D.-X.; Dang, Y.-M.; Zhang, Q. PI3K–AKT Pathway Protects Cardiomyocytes Against Hypoxia-Induced Apoptosis by MitoKATP-Mediated Mitochondrial Translocation of pAKT. *Cell Physiol. Biochem.* **2018**, *49*, 717–727. https://doi.org/10.1159/000493037.

8. Zhang, Y.; Gui, Y.; Belke, D.; Wang, X.; Su, W.; Liu, M.; Yan, B.; Sun, J.; Hu, X.; Zheng, X.-L. Monomethyl Fumarate Confers Cardioprotection after Myocardial Infarction via HCAR2-Dependent Activation of PI3K/Akt Signaling. *Cell Death Discov.* **2025**, *12*, 63. https://doi.org/10.1038/s41420-025-02927-6.
9. Ma, X.; Gao, L.; Ge, R.; Yuan, T.; Lin, B.; Zhen, L. CDC-like Kinase 3 Deficiency Aggravates Hypoxia-Induced Cardiomyocyte Apoptosis through AKT Signaling Pathway. *Vitr. Cell. Dev. Biol.-Anim.* **2024**, *60*, 333–342. https://doi.org/10.1007/s11626-024-00886-3.
10. Zheng, K.; Zhang, Q.; Lin, G.; Li, Y.; Sheng, Z.; Wang, J.; Chen, L.; Lu, H. Activation of Akt by SC79 Protects Myocardiocytes from Oxygen and Glucose Deprivation (OGD)/Re-Oxygenation. *Oncotarget* **2017**, *8*, 14978–14987. https://doi.org/10.18632/oncotarget.14785.
11. Khosravi, F.; Ahmadvand, N.; Bellusci, S.; Sauer, H. The Multifunctional Contribution of FGF Signaling to Cardiac Development, Homeostasis, Disease and Repair. *Front. Cell Dev. Biol.* **2021**, *9*, 672935. https://doi.org/10.3389/fcell.2021.672935.
12. Kaur, N.; Gare, S.R.; Ruiz-Velasco, A.; Miller, J.M.; Abouleisa, R.R.E.; Ou, Q.; Shen, J.; Soran, H.; Mohamed, T.M.A.; Liu, W. FGF21/FGFR1-β-KL Cascade in Cardiomyocytes Modulates Angiogenesis and Inflammation under Metabolic Stress. *Heliyon* **2023**, *9*, e14952. https://doi.org/10.1016/j.heliyon.2023.e14952.
13. Li, J.; Liu, H.; Srivastava, S.P.; Hu, Q.; Gao, R.; Li, S.; Kitada, M.; Wu, G.; Koya, D.; Kanasaki, K. Endothelial FGFR1 (Fibroblast Growth Factor Receptor 1) Deficiency Contributes Differential Fibrogenic Effects in Kidney and Heart of Diabetic Mice. *Hypertension* **2020**, *76*, 1935–1944. https://doi.org/10.1161/HYPERTENSIONAHA.120.15587.
14. Chen, L.; Zheng, L.; Qin, Y.; Liu, B.; Zheng, Y.; Tong, X.; Dai, M.; Gong, G. FGF21-FGFR1 Signaling Protects against Cardiac Hypertrophy by Regulating PINK1-Mediated Mitophagy Pathway. *J. Adv. Res.* **2026**, *85*, 1009–1023. https://doi.org/10.1016/j.jare.2025.10.053.
15. Matsiukevich, D.; House, S.L.; Weinheimer, C.; Kovacs, A.; Ornitz, D.M. Fibroblast Growth Factor Receptor Signaling in Cardiomyocytes Is Protective in the Acute Phase Following Ischemia-Reperfusion Injury. *Front. Cardiovasc. Med.* **2022**, *9*, 1011167. https://doi.org/10.3389/fcvm.2022.1011167.
16. Ulm, S.; Liu, W.; Zi, M.; Tsui, H.; Chowdhury, S.K.; Endo, S.; Satoh, Y.; Prehar, S.; Wang, R.; Cartwright, E.J.; et al. Targeted Deletion of ERK2 in Cardiomyocytes Attenuates Hypertrophic Response but Provokes Pathological Stress Induced Cardiac Dysfunction. *J. Mol. Cell. Cardiol.* **2014**, *72*, 104–116. https://doi.org/10.1016/j.yjmcc.2014.03.002.
17. Ruiz-Velasco, A.; Zi, M.; Hille, S.S.; Azam, T.; Kaur, N.; Jiang, J.; Nguyen, B.; Sekeres, K.; Binder, P.; Collins, L.; et al. Targeting Mir128-3p Alleviates Myocardial Insulin Resistance and Prevents Ischemia-Induced Heart Failure. *eLife* **2020**, *9*, e54298. https://doi.org/10.7554/eLife.54298.
18. Zhou, Y.; Wu, C.; Lu, G.; Hu, Z.; Chen, Q.; Du, X. FGF/FGFR Signaling Pathway Involved Resistance in Various Cancer Types. *J. Cancer* **2020**, *11*, 2000–2007. https://doi.org/10.7150/jca.40531.
19. Chang, S.C.; Ren, S.; Rau, C.D.; Wang, J.J. Isoproterenol-Induced Heart Failure Mouse Model Using Osmotic Pump Implantation. In *Experimental Models of Cardiovascular Diseases*; Ishikawa, K., Ed.; Methods in Molecular Biology; Springer New York: New York, NY, USA, 2018; Volume 1816, pp. 207–220 ISBN 978-1-4939-8596-8.
20. Jo, H.; Mondal, S.; Tan, D.; Nagata, E.; Takizawa, S.; Sharma, A.K.; Hou, Q.; Shanmugasundaram, K.; Prasad, A.; Tung, J.K.; et al. Small Molecule-Induced Cytosolic Activation of Protein Kinase Akt Rescues Ischemia-Elicited Neuronal Death. *Proc. Natl. Acad. Sci. U. S. A.* **2012**, *109*, 10581–10586. https://doi.org/10.1073/pnas.1202810109.
21. Chu, N.; Le, N.; Nebie, O.; Yang, S. Structural and Mechanistic Basis of mTORC2 Activation of Protein Kinase AKT/PKB. *Biochem. J.* **2026**, *483*, 375–389. https://doi.org/10.1042/BCJ20253108.
22. Taylor, M.S.; Chen, M.; Hancock, M.; Wranik, M.; Miller, B.D.; O'Meara, T.R.; Palanski, B.A.; Ficarro, S.B.; Groendyke, B.J.; Xiang, Y.; et al. Structural Basis for the Recruitment and Selective Phosphorylation of Akt by mTORC2. *Science* **2026**, *391*, eadv7111. https://doi.org/10.1126/science.adv7111.
23. Toth, M.J.; Ward, K.; Van Der Velden, J.; Miller, M.S.; VanBuren, P.; LeWinter, M.M.; Ades, P.A. Chronic Heart Failure Reduces Akt Phosphorylation in Human Skeletal Muscle: Relationship to Muscle Size and Function. *J. Appl. Physiol.* **2011**, *110*, 892–900. https://doi.org/10.1152/japplphysiol.00545.2010.
24. Kapustian, L.; Kroupskaya, I.; Rozhko, O.; Bobyk, V.; Ryabenko, D.; Sidorik, L. Akt1 Expression and Activity at Different Stages in Experimental Heart Failure. *Pathophysiology* **2014**, *21*, 147–151. https://doi.org/10.1016/j.pathophys.2013.11.005.
25. Chaanine, A.H.; Hajjar, R.J. AKT Signalling in the Failing Heart. *Eur. J. Heart Fail.* **2011**, *13*, 825–829. https://doi.org/10.1093/eurjhf/hfr080.
26. Turner, N.; Grose, R. Fibroblast Growth Factor Signalling: From Development to Cancer. *Nat. Rev. Cancer* **2010**, *10*, 116–129. https://doi.org/10.1038/nrc2780.

27. Manning, B.D.; Toker, A. AKT/PKB Signaling: Navigating the Network. *Cell* **2017**, *169*, 381–405. https://doi.org/10.1016/j.cell.2017.04.001.
28. Matsui, T.; Tao, J.; Del Monte, F.; Lee, K.-H.; Li, L.; Picard, M.; Force, T.L.; Franke, T.F.; Hajjar, R.J.; Rosenzweig, A. Akt Activation Preserves Cardiac Function and Prevents Injury After Transient Cardiac Ischemia In Vivo. *Circulation* **2001**, *104*, 330–335. https://doi.org/10.1161/01.CIR.104.3.330.
29. Völkers, M.; Konstandin, M.H.; Doroudgar, S.; Toko, H.; Quijada, P.; Din, S.; Joyo, A.; Ornelas, L.; Samse, K.; Thuerauf, D.J.; et al. Mechanistic Target of Rapamycin Complex 2 Protects the Heart From Ischemic Damage. *Circulation* **2013**, *128*, 2132–2144. https://doi.org/10.1161/CIRCULATIONAHA.113.003638.
30. Moschella, P.C.; McKillop, J.; Pleasant, D.L.; Harston, R.K.; Balasubramanian, S.; Kuppuswamy, D. mTOR Complex 2 Mediates Akt Phosphorylation That Requires PKCε in Adult Cardiac Muscle Cells. *Cell. Signal.* **2013**, *25*, 1904–1912. https://doi.org/10.1016/j.cellsig.2013.05.001.
31. Miyamoto, S.; Purcell, N.H.; Smith, J.M.; Gao, T.; Whittaker, R.; Huang, K.; Castillo, R.; Glembotski, C.C.; Sussman, M.A.; Newton, A.C.; et al. PHLPP-1 Negatively Regulates Akt Activity and Survival in the Heart. *Circ. Res.* **2010**, *107*, 476–484. https://doi.org/10.1161/CIRCRESAHA.109.215020.
32. Deng, Y.; Huang, X.; Hu, Y.; Zhong, W.; Zhang, H.; Mo, C.; Wang, H.; Ding, B.-S.; Wang, C. Deficiency of Endothelial FGFR1 Signaling via Upregulation of ROCK2 Activity Aggravated ALI/ARDS. *Front. Immunol.* **2023**, *14*, 1041533. https://doi.org/10.3389/fimmu.2023.1041533.
33. Tahara, N.; Akiyama, R.; Wang, J.; Kawakami, H.; Bessho, Y.; Kawakami, Y. The FGF-AKT Pathway Is Necessary for Cardiomyocyte Survival for Heart Regeneration in Zebrafish. *Dev. Biol.* **2021**, *472*, 30–37. https://doi.org/10.1016/j.ydbio.2020.12.019.
34. Frangogiannis, N.G. The Extracellular Matrix in Ischemic and Nonischemic Heart Failure. *Circ. Res.* **2019**, *125*, 117–146. https://doi.org/10.1161/CIRCRESAHA.119.311148.
35. Piek, A.; De Boer, R.A.; Silljé, H.H.W. The Fibrosis-Cell Death Axis in Heart Failure. *Heart Fail. Rev.* **2016**, *21*, 199–211. https://doi.org/10.1007/s10741-016-9536-9.
36. Heinzel, F.R.; Hohendanner, F.; Jin, G.; Sedej, S.; Edelmann, F. Myocardial Hypertrophy and Its Role in Heart Failure with Preserved Ejection Fraction. *J. Appl. Physiol.* **2015**, *119*, 1233–1242. https://doi.org/10.1152/japplphysiol.00374.2015.
37. Shiojima, I.; Schiekofer, S.; Schneider, J.G.; Belisle, K.; Sato, K.; Andrassy, M.; Galasso, G.; Walsh, K. Short-Term Akt Activation in Cardiac Muscle Cells Improves Contractile Function in Failing Hearts. *Am. J. Pathol.* **2012**, *181*, 1969–1976. https://doi.org/10.1016/j.ajpath.2012.08.020.
38. Erny, E.; Koentges, C.; Mukherjee, D.; Wirth, L.; Kamaras, C.; Zell, F.; Hossfeld, M.; Groß, O.; Lother, A. Downregulation of TCF19 and ATAD2 Causes Endothelial Cell Cycle Arrest at the Transition from Cardiac Hypertrophy to Heart Failure. *Basic. Res. Cardiol.* **2025**, *120*, 1209–1224. https://doi.org/10.1007/s00395-025-01139-4.
39. Wang, M.; Han, X.; Wang, Q.; Yu, T.; Luo, W.; Ye, S.; Guo, X.; Xu, Z.; Huang, Z.; Min, J.; et al. Checkpoint Kinase Wee1 Activation Drives Inflammation and Hypertrophy through the Protein Kinase B/Phosphoinositide 3-Kinases–Nuclear Factor κB Pathway in Cardiomyocytes. *Eur. Heart J.* **2026**, *47*, 1702–1717. https://doi.org/10.1093/eurheartj/ehaf349.
40. Livak, K.J.; Schmittgen, T.D. Analysis of Relative Gene Expression Data Using Real-Time Quantitative PCR and the 2−ΔΔCT Method. *Methods* **2001**, *25*, 402–408. https://doi.org/10.1006/meth.2001.1262.
41. Fonseka, O.; Raja, R.; Ross, C.; Gare, S.R.; Zhang, J.; Hille, S.S.; King, K.; Ruiz-Velasco, A.; Kaur, N.; Chen, X.; et al. XBP1s-EDEM2 Prevents the Onset and Development of HFpEF by Ameliorating Cardiac Lipotoxicity. *Circulation* **2025**, *151*, 1583–1605. https://doi.org/10.1161/CIRCULATIONAHA.124.072194.
42. Tang, D.; Chen, M.; Huang, X.; Zhang, G.; Zeng, L.; Zhang, G.; Wu, S.; Wang, Y. SRplot: A Free Online Platform for Data Visualization and Graphing. *PLoS ONE* **2023**, *18*, e0294236. https://doi.org/10.1371/journal.pone.0294236.
43. Ruiz-Velasco, A.; Raja, R.; Chen, X.; Ganenthiran, H.; Kaur, N.; Alatawi, N.H.O.; Miller, J.M.; Abouleisa, R.R.E.; Ou, Q.; Zhao, X.; et al. Restored Autophagy Is Protective against PAK3-Induced Cardiac Dysfunction. *iScience* **2023**, *26*, 106970. https://doi.org/10.1016/j.isci.2023.106970.

Disclaimer/Publisher's Note: The statements, opinions and data contained in all publications are solely those of the individual author(s) and contributor(s) and not of MDPI and/or the editor(s). MDPI and/or the editor(s) disclaim responsibility for any injury to people or property resulting from any ideas, methods, instructions or products referred to in the content.